PolyPublie
Polytechnique Montréal

POLYTECHNIQUE MONTRÉAL
UNIVERSITÉ D'INGÉNIERIE

Titre: Title:	Therapeutic Magnetic Microcarriers Characterization by Measuring Magnetophoretic Attributes
Auteur: Author:	Guillermo Vidal Ibacache
Date:	2013
Type:	Mémoire ou thèse / Dissertation or Thesis
Référence: Citation:	Vidal Ibacache, G. (2013). Therapeutic Magnetic Microcarriers Characterization by Measuring Magnetophoretic Attributes [Mémoire de maîtrise, École Polytechnique de Montréal]. PolyPublie. https://publications.polymtl.ca/1171/

Document en libre accès dans PolyPublie
Open Access document in PolyPublie

URL de PolyPublie: PolyPublie URL:	https://publications.polymtl.ca/1171/
Directeurs de recherche: Advisors:	Sylvain Martel
Programme: Program:	Génie informatique

Ce fichier a été téléchargé à partir de PolyPublie, le dépôt institutionnel de Polytechnique Montréal
This file has been downloaded from PolyPublie, the institutional repository of Polytechnique Montréal

https://publications.polymtl.ca

UNIVERSITÉ DE MONTRÉAL

THERAPEUTIC MAGNETIC MICROCARRIERS CHARACTERIZATION BY MEASURING MAGNETOPHORETIC ATTRIBUTES

GUILLERMO VIDAL IBACACHE

DÉPARTEMENT DE GÉNIE INFORMATIQUE ET GÉNIE LOGICIEL

ÉCOLE POLYTECHNIQUE DE MONTRÉAL

MÉMOIRE PRÉSENTÉ EN VUE DE L'OBTENTION

DU DIPLÔME DE MAÎTRISE ÈS SCIENCES APPLIQUÉES

(GÉNIE INFORMATIQUE)

AOÛT 2013

© Guillermo Vidal Ibacache, 2013.

UNIVERSITÉ DE MONTRÉAL

ÉCOLE POLYTECHNIQUE DE MONTRÉAL

Ce mémoire intitulé:

THERAPEUTIC MAGNETIC MICROCARRIERS CHARACTERIZATION BY MEASURING MAGNETOPHORETIC ATTRIBUTES

présenté par : VIDAL IBACACHE Guillermo

en vue de l'obtention du diplôme de : Maîtrise ès sciences appliquées

a été dûment accepté par le jury d'examen constitué de :

M. LANGLOIS J.M. Pierre, Ph.D., président

M. MARTEL Sylvain, Ph.D., membre et directeur de recherche

M. COHEN-ADAD Julien, Ph.D., membre

DEDICATION

To my beloved wife Rosita, and my kids Gabriel and Alonso...

ACKNOWLEDGEMENT

First of all, I appreciate the support that my research supervisor, Mr. Sylvain Martel, provided me during my journey in the NanoRobotics Laboratory. He was able to give me fresh insights when I went to him asking for advice. He is able to put the right questions in the right moment and to explain the more complex problems in very simple words, without his constant push and help this project would not have seen an end.

Working environment in the laboratory has been exceptional and, in my opinion, one of the major reasons for this is the presence of Mr. Charles Tremblay. He is energetic, joyful, an excellent professional, always willing to help and teach; and it is always a pleasure to talk to him on any subject.

Thanks to Ke Peng and Behnam Izadi, we spent a lot of time together setting up experiences that later were useful to do my own work. Ke is kind and warm, sharp-eyed and is always prompt to give help. Behnam is quiet, introverted, and hardworking; thanks to his work I was able to initially see the movement of aggregations in my experiments.

To Ms. Neila Kaou, who is always willing to listen and helped me with plans and some administrative stuff.

To Manuel Vonthron, head of the computer team who is always doing things really quickly and right with the enthusiasm of the youth. He is also always available to provide careful feedback.

To Viviane Lalande, who set a high bar to everyone in the lab with her excellent work and leadership.

To Alexander Bigot, talking to him is always a way to see the things with another prism, which is usually simpler than my tendency to complicate things.

To J.B. Mathieu, who spent a Saturday evening to explain to me how he was able to inject particles and did his incredible job with magnetic microparticles aggregations. He took time from his vacations to help me.

To Nina Olaemei, who helped me with the nightmare of trying to get a working microfluidic channel.

To all other members of the laboratory, who received me and were patient to my communication problems in English and especially in French.

Lastly, thanks to my family, my wife and kids that have been here all this time, dealing with my mood changes and supporting me with their love.

Porque no tenemos nada, queremos hacerlo todo...

- Carlos Dittborn

Alepue mapu küpan pian

amulen, amulen

alüpu puan

doy ayeple wanglen.

Vengo de las tierras de Alepue, diré

avanzo, avanzo

quiero llegar muy lejos

más allá del umbral de las estrellas.

- Leonel Lienlaf

ABSTRACT

Micro/nano robots are considered a promising approach to conduct minimally invasive interventions. We have proposed to embed magnetic nanoparticles in therapeutic or diagnostic agents in order to magnetically control them. A modified clinical Magnetic Resonance Imaging (MRI) scanner is used to provide the driving force that allows these magnetically embedded microcarriers to navigate the vascular human network. By using specific Magnetic Resonance (MR) gradient sequences this method has been validated in previous research works.

Magnetophoresis is the term used to describe the fact that a magnetic particle changes its trajectory under the influence of a magnetic force while being carried by a fluid flow. This movement depends on the particle's magnetic characteristics, the particle's geometric shape, the fluid flow's attributes and other factors. In our proposed method, magnetic microcarriers can be produced in several different ways, and so their response will differ to the same magnetic force and fluid flow conditions. The outcome of the therapeutic treatment using our method depends on the adequate selection of the therapeutic and/or diagnosis agents to be used. The selected therapeutic and/or diagnosis magnetic microcarrier also influences the selection of the MR gradient sequence that best fit for a given treatment.

This master's thesis presents the design of a device intended to assess the magnetophoretic properties of magnetic therapeutic microcarriers and/or diagnostic agents. Such characterization is essential for determining the optimal sequences of magnetic gradients to deflect their trajectory through relatively complex vascular networks in order to reach a pre-defined target. A microfluidic device was fabricated to validate the design. Magnetophoretic velocities are measured and a simple tracking method is proposed. The preliminary experimental results indicate that, despite some limitations, the proposed technique has the potential to be appropriate to characterize any drug and/or diagnosis magnetic microcarrier containing different magnetic nanoparticle content.

RÉSUMÉ

Des micro/nano-robots sont considérés comme une approche prometteuse pour mener des interventions minimalement invasives. Nous avons proposé d'intégrer des nanoparticules magnétiques dans des agents thérapeutiques ou de diagnostic afin de les contrôler magnétiquement. Un scanner d'imagerie par résonance magnétique (IRM) clinique modifié est utilisé afin de fournir la force motrice qui permet à ces microporteurs magnétiques à naviguer dans le réseau vasculaire humain. En utilisant des séquences spécifiques des gradients de résonance magnétique (MR) cette méthode a été validée dans des travaux de recherche antérieurs.

Magnétophorèse est le terme utilisé pour décrire le fait qu'une particule magnétique modifie sa trajectoire sous l'influence d'une force magnétique tout en étant portée par un flux de fluide. Ce mouvement dépend des caractéristiques de la particule magnétique, de sa forme géométrique, des attributs de l'écoulement de fluide et d'autres facteurs. Dans notre méthode proposée, les microporteurs magnétiques peuvent être réalisés de différentes manières, et donc leur réponse sera différente à la même force magnétique et dans les mêmes conditions d'écoulement de fluide. Le résultat du traitement thérapeutique utilisant notre méthode dépend de la sélection adéquate des agents thérapeutiques et/ou de diagnostic à utiliser. Le microporteur magnétique thérapeutique et /ou de diagnostic choisi influe également sur le choix de la séquence des gradients magnétiques que meilleur se ajustement pour un traitement donné.

Ce mémoire de maîtrise présente la conception d'un dispositif destiné à évaluer les propriétés magnétophorétiques des agents microporteurs magnétiques thérapeutiques et/ou de diagnostic. Une telle caractérisation est essentielle pour déterminer les séquences optimales des gradients magnétiques pour dévier leur trajectoire à travers des réseaux vasculaires relativement complexes dans le but d'atteindre un objectif prédéfini. Un dispositif microfluidique est fabriqué pour valider la conception. Las vitesses magnétophorétiques sont mesurées et une méthode de suivi simple est proposée. Les résultats des experiences préliminaires indiquent que, malgré certaines limitations, la technique proposée a le potentiel d'être approprié pour caractériser n'importe quel microporteur magnétique thérapeutique et/ou de diagnostic contenant différents taux de nanoparticules magnétiques.

CONTENTS

DEDICATION... III

ACKNOWLEDGEMENT IV

ABSTRACT…. VI

RÉSUMÉ…. VII

CONTENTS…. VIII

LIST OF TABLES XI

LIST OF FIGURES XII

LIST OF SYMBOLS AND ABBREVIATIONS XV

LIST OF APPENDICES XVI

CHAPTER 1 INTRODUCTION 1

1.1 Background and motivation 1

1.2 Problem statement 2

1.2.1 Thesis objectives 2

1.3 Overview of the thesis 3

CHAPTER 2 LITERATURE REVIEW 5

2.1 Magnetophoresis 5

2.1.1 Magnetism basic concepts 5

2.1.2 Magnetic force 7

2.1.3 Microfluidics basics 8

2.1.4 Magnetophoretic trajectory observation 9

2.2 Magnetic Manipulation 11

2.3 Magnetic Resonance Navigation 12

2.4 Object tracking 14

2.4.1 Particle Tracking 16

CHAPTER 3 OVERVIEW OF THE APPROACH 19

3.1 Microfluidic design 20

3.1.1 Relevant physics principles 20

3.1.2 Biological considerations 23

3.1.3 Chamber 25

3.2 Microparticles 30

3.3 Simulations 30

3.4 Experiments 34

3.4.1 General setup 34

3.4.2 Experimental results 35

3.5 Tracking tool 35

CHAPTER 4 MEASURING THE MAGNETOPHORETIC CHARACTERISTICS OF MAGNETIC AGENTS FOR TARGETED DIAGNOSTIC OR THERAPEUTIC INTERVENTIONS IN THE VASCULAR NETWORK 38

4.1 Title Page 38

4.2 Abstract 39

4.3 Introduction 39

4.4 Theoretical background 41

4.4.1 Particle movement 41

4.4.2 Particle tracking algorithm 43

4.5 Experiments 43

4.5.1 Microparticles for magnetophoresis measurements 43

4.5.2 Microfluidic design and fabrication 43

4.5.3 Experimental setup 45

4.6 Results 45
4.6.1 Experiments results 45
4.6.2 Tracking experiments 47
4.7 Discussion 48
4.8 Conclusions and future work 49
4.9 Acknowledgments 50
CHAPTER 5 PROPOSED TRACKING METHOD 51
5.1 Tracking using OpenCV blobtrack 51
5.2 Tracking tool description 55
5.2.1 Frame processing 57
5.2.2 Motion estimation 60
5.2.3 Location accuracy 63
CHAPTER 6 GENERAL DISCUSSION 65
6.1 Experimental setup 65
6.2 Data acquisition software 69
CHAPTER 7 CONCLUSION 71
REFERENCES 73

LIST OF TABLES

Table 3-1 Simulation parameters 32

LIST OF FIGURES

Figure 2-1 CTV method schematics. Cells identified in the five consecutive frames are named t_1 to t_5 respectively. The search area between frames is determined by radius *r*. A predicted location of the cell in frame 3 is indicated as *p*. The real cell path is depicted in green. 18

Figure 3-1 Schematic diagram of a general MRN procedure. 20

Figure 3-2 Free body diagram. Forces on a magnetic particle (green sphere in the center) in the magnetophoretic chamber are depicted. The fluid flow is in *x* direction. Magnetic force is applied in *y* direction. In *z* direction acts gravity and buoyancy. Drag force resist movement in all directions. 21

Figure 3-3 Schematic representation of human cardiovascular system vessels. Vessels' main parameters depicted are inner diameter, average blood flow speed and Reynolds number adapted from [72]. 24

Figure 3-4 Bending problem in the initial chamber design. (a) Without magnetic steering force applied. Magnetic microparticles are represented in blue. Stream-lines are represented by blue arrows crossing the chamber. The bending zone is indicated in the middle of the chamber. (b) Expected effect on a magnetic aggregation when the magnetic force is applied. The expected deflection trajectory is shown in red; the effect of the bending zone on deflection pattern is shown in green. 26

Figure 3-5 Schematics of fluid flow streamlines in channel connections. (a) Schematics of fluid flow streamlines for right angle channel connection with vortex roll forming at the entrance of the magnetophoretic chamber (adapted from [16]). (b) Schematic of smoothed fluid flow by using angle connection. 27

Figure 3-6 Flow pattern in the magnetophoretic chamber. Flow observed in the magnetophoretic chamber when ink is pumped in the microparticles inlet and DI water in the main flow inlet. 29

Figure 3-7 Simulated individual microparticle's deflection patterns. Flow velocities considered are 20.8, 10.4, 5.2 and 2.6 mm/s (from top to bottom in the graphic). 32

Figure 3-8 Simulated microparticles aggregations deflection patterns. Flow velocities considered are 20.8, 10.4, 5.2 and 2.6 mm/s (from top to bottom in the graphic). 33

Figure 4-1 Schematic of the microfluidic device design. The complete device is 200 μm deep. Magnetophoretic chamber is 7 mm × 6 mm. Main flow and microparticles flow meet in the 2 mm entrance channel.....44

Figure 4-2 Schematic of the experimental setup. Prop Coil 1 and Prop Coil 2 refer to the custom Maxwell pair coils. It is seen that the fluid flow and magnetic gradient are intended to be orthogonal. Then all movement perpendicular to the flow is solely produced by the magnetic gradient from the propulsion coils. 46

Figure 4-3 Effect of the fluid flow velocity on the deflection pattern of magnetic microparticles aggregations moving along the magnetophoretic chamber, in (a) the fluid velocity is 20.8 mm/s and it is difficult to notice the deflection of microparticles; in (b) the fluid velocity is 10.4 mm/s; in (c) fluid velocity is 5.2 mm/s, and in (d) it is set to 2.6 mm/s 46

Figure 4-4 Comparison between the tracking software applied to raw video (left side) and to filtered frames video (right side). Only for the slower fluid velocity is possible to extract directly from raw video the trajectory of magnetic microparticle aggregations.....47

Figure 5-1 Distance measurement to detect blob intersection. The quantities $d_1 = x_2 - x_1$ and $d_2 = y_2 - y_1$ are horizontal and vertical distances between centroids of the blobs, w_1, w_2 are the widths and h_1, h_2 are the heights of the blobs respectively. If $d_1 < (w_1/2 + w_2/2) \wedge d_2 < (h_1/2 + h_2/2)$ the blobs are considered merged. 52

Figure 5-2 Detected aggregations in different frames. Accumulated detected particles at different points in time are shown at left. Foreground resulted by background subtraction from current frame is shown at the right. The video used is the one at which the fluid velocity is 2.6 mm/s. Particles detected are highlighted with a circle surrounding them.....53

Figure 5-3 Filtering process example applied on the same frames as in Figure 5-2. The tracked aggregation is highlighted by encircling it to show the effect of each filter step.....54

Figure 5-4 Window to enter fluid flow speed used in the opened video. 55

Figure 5-5 Spatial calibration. Selection of a region of known horizontal size that is used to calculate the equivalent size in pixels, in this case the result is 27 pixels/mm. 56

Figure 5-6 Tracking region selection. The user can define the region in which the tracking is to be performed. 57

Figure 5-7 Simple flowchart of the preliminary tracking software. 58

Figure 5-8 Image processing prior to tracking. 59

Figure 5-9 Deflection pattern of aggregations in 2.6 mm/s movie. 62

Figure 5-10 Deflection pattern of aggregations in 5.2 mm/s movie. 62

Figure 6-1 Prolate ellipsoid representing magnetic chain-like aggregation shape. 66

Figure 6-2 Current chamber design problem. Aggregations represented in blue are subjected to the magnetic gradient at the right time. In green is represented the situation when the magnetic gradient is turned on too early. 68

LIST OF SYMBOLS AND ABBREVIATIONS

CTV	Cell Tracking Velocimetry
DI	De-ionized
HGMS	High Gradient Magnetic Separation
MR	Magnetic Resonance
MRI	Magnetic Resonance Imaging
MRN	Magnetic Resonance Navigation
MR-Sub	Magnetic Resonance Submarine
MRT	Magnetic Resonance Targeting
MTTM	Magnetophoretic Trajectory Tracking Magnetometry
PMMA	Polymethyl methacrylate
TMMC	Therapeutic Magnetic Micro Carriers
SI	International System of Units (from French: Le Système International d'Unités)

LIST OF APPENDICES

APPENDIX 1– Rod model for chain-like magnetic aggregations.....83

CHAPTER 1 INTRODUCTION

1.1 Background and motivation

Minimally invasive interventions are attracting a lot of interest in the research community, mainly due to the advantages of this kind of interventions: reduced patient recovery time, shorter stay in the hospital and fewer complications. In the context of the Magnetic Resonance Submarine (MR-Sub) project a new minimally invasive technique for cancer treatment and diagnosis, called Magnetic Resonance Navigation (MRN), has been proposed. This technique is based on the use of the main magnetic homogeneous field and the magnetic gradients of an upgraded Magnetic Resonance Imaging (MRI) scanner in order to navigate therapeutic or diagnostic agents with embedded magnetic nanoparticles to target specific locations in the vascular human network.

Most of current cancer treatments involving drug administration are systemic, which means that the drugs are delivered in the bloodstream causing them to affect cells all over the organism with just around 1% or less destroying tumor cells [1, 2]. The MRN technique is expected to produce a significant increase in targeting efficiency and the feasibility of this method has already been demonstrated [3] by our research group.

A major challenge faced in this technique is the fact that the human vasculature is very complex and heterogeneous with vessels ranging from some millimeters (major arteries) to a few micrometers (arterioles, capillaries) in diameter. To accommodate the smaller human body vessels, the drug carrier size must be reduced, which in turn reduces the amount of drug that can be transported. On the other hand, smaller carriers are more difficult to be navigated due to its reduced magnetic volume.

In [4, 5] it was demonstrated that it is possible to produce a drug carrier of about 50 μm in diameter size to target a tumor deep inside the body. However, in [6] the authors noticed that normal MRI gradient coils were not sufficient to allow steering of magnetic microcarriers in a Y-shaped bifurcation, then upgraded gradient coils were tested and validated. In this last study it was also stated that, in order to improve steering efficiency, it could be exploited the fact that

magnetic microcarriers tend to agglomerate when being used as therapeutic and/or diagnosis vectors.

For improving targeting efficiency by using the aggregation of magnetic microcarriers we are obligated to understand and evaluate the response of these aggregations when subjected to magnetic gradients. In different given conditions of fluid flow and magnetic force, magnetic microparticle aggregations show different deflection patterns. Thus the study of this deflection patterns gives clues on the magnetic response of them. Hence, by evaluating deflection patterns the magnetophoretic velocity of these entities can be estimated and used to predict their behavior in treatment conditions.

Moreover, in [7] it has been published that even for magnetic microspheres of the same size prepared under the same conditions, magnetophoretic velocities can differ by a factor of 4 or more. This emphasizes the need for an instrument to estimate magnetic microcarriers response to magnetic gradients when designed to be used in targeted drug delivery and/or diagnosis applications in the context of MRN treatments.

1.2 Problem statement

The main goal of the MR-Sub project is to develop a platform capable of navigating magnetic microcarriers in the human cardiovascular system according to a pre-defined pathway.

1.2.1 Thesis objectives

The objective of this thesis is to design a device in order to collect data on the magnetic response of the microcarriers when used in MRN. To attain this objective the main goal is divided in the following sub-goals:

- design a microfluidic chamber in order to allow the magnetic microcarriers to move while following the fluid flow,
- record microparticles' course when subjected to a magnetic steering force perpendicular to the direction of the flow.

- estimate the magnetophoretic velocity of magnetic particles, that in turn, should allow estimating the trajectory that a microcarrier would follow under similar circumstances.

Main contributions of the work for this thesis are:

- a conference paper presented in the 3M-NANO 2012 Conference (International Conference on Manipulation, Manufacturing and Measurement on the Nanoscale) in Xi'an, China under the title: *"Characterization by magnetophoresis of therapeutic microcarriers relying on embedded nanoparticles to allow navigation in the vascular network"* [70]; this work was selected as a Best Conference Paper Award Finalist.
- a journal paper published in 2013 in the Journal of Micro-Bio Robotics as: G. Vidal and S. Martel, "*Measuring the magnetophoretic characteristics of magnetic agents for targeted diagnostic or therapeutic interventions in the vascular network*" [10] .
- a microfluidics chamber design for magnetophoretic experiences.
- a basic software tracking tool tailored for the conditions of the magnetophoretic experiences performed.

Unless the contrary is indicated, the developments presented in this document are the contribution of the author. Exceptions are indicated and mainly are: OpenCV blobtrack modified application that was adapted by Behnam Izadi for experiences in Ke Peng's master thesis work [8] and Joerg Buchholz's Particle System Toolbox [9] used for magnetic microparticles movement simulations.

1.3 Overview of the thesis

The thesis organization is as follows: in the first chapter the background, motivation and problem statement are presented; in Chapter 2 there is a literature review on the way in which the trajectory of magnetic particles has been studied before and its previous applications; in Chapter 3 the approach used in this work is presented; in Chapter 4 the published paper [10] showing the preliminary results of the selected design in its original version is introduced; Chapter 5 introduces the proposed tracking method based on finding presented in Chapter 4; Chapter 6

presents a general discussion of this work; finally Chapter 7 summarizes the project and presents future perspectives for it.

CHAPTER 2 LITERATURE REVIEW

Retrieving data on the reactivity shown by MR navigable microcarriers seems to be fundamental in order to determine optimal control sequences during MRN treatments. This chapter focuses on providing an overview of previous work on the techniques for observing magnetic microparticles' trajectories, on the importance of aggregations in the context of MRN and the need for a method to estimate compared drug/diagnosis magnetic microcarriers performance. On the basis of this review the main advances in the area are highlighted.

2.1 Magnetophoresis

The study of the movement of magnetic particles in a fluid induced by the influence of a magnetic field (termed as magnetophoresis) has been the object of research in several works. As early as in 1960, an apparatus was proposed to measure the magnetic susceptibility of single particles by determining the velocity that particles get when in an inhomogeneous magnetic field [11]. This apparatus used a microscope to observe a particle's trajectory and a stop watch to time the movement and then estimate the particle's assumed velocity.

2.1.1 Magnetism basic concepts

In order to understand magnetophoresis, some basic definitions on magnetism in materials are required.

The magnetic induction, $\mathbf{B}$[1], is the response of a given material to an applied magnetic field, $\mathbf{H}$. The relationship between $\mathbf{B}$ and $\mathbf{H}$ is given by (in SI units):

$$\boldsymbol{B} = \mu_0(\boldsymbol{H} + \boldsymbol{M}) \qquad 2\text{-}1$$

[1] In this document bold letters indicate vectors : for example $\boldsymbol{A}$ is a vector and A is a scalar indicating the magnitude of vector $\mathbf{A}$.

where μ_0 is the permeability in free space and **M** is the magnetization induced inside the material and is dependent on the characteristics of it. The magnetization is defined as the magnetic moment per unit volume

$$\boldsymbol{M} = \frac{\boldsymbol{m}}{V} \qquad 2\text{-}2$$

where $\boldsymbol{m}$ is the dipole magnetic moment and V is the volume of the magnetic material. The magnetic moment relates to the torque that is exerted on a magnet dipole or a current loop when a magnetic field is applied. The dipole magnetic moment of a material depends mainly on orbital and spin magnetic moments of the electrons in the constituent atoms of it.

The magnetic susceptibility of a material is defined by

$$\chi = \frac{\boldsymbol{M}}{\boldsymbol{H}} \qquad 2\text{-}3$$

The susceptibility is an indication of the responsiveness of a material to an applied magnetic field. Magnetization curves are built by plotting **M** versus **H** (or **B** versus **H**), and are used to identify the magnetic type of material.

The magnetic permeability is defined by

$$\mu = \frac{\boldsymbol{B}}{\boldsymbol{H}} \qquad 2\text{-}4$$

and indicates how permeable a material is to the applied magnetic field.

Permeability μ and susceptibility χ (in SI units) are related by

$$\mu = \mu_0(1 + \chi) \qquad 2\text{-}5$$

with μ_0 the permeability in free space.

Materials are classified as diamagnetic, paramagnetic, antiferromagnetic, ferrimagnetic and ferromagnetic depending on their magnetic characteristics. For diamagnetic, paramagnetic and antiferromagnetic materials, magnetization curves are linear; a relatively large applied field is required to produce changes in magnetization and there is no remanent magnetization if the applied field is removed. For ferrimagnetic and ferromagnetic materials, magnetization curves have the typical hysteresis loop form; there is a magnetization saturation point after which

negligible change is produced in magnetization by increasing the applied field and removing the applied field does not reduce magnetization to zero (if saturation has been reached), this remanent magnetization has several technological applications [12].

2.1.2 Magnetic force

When an inhomogeneous magnetic field is applied to a particle, this magnetic field exerts a force on the particle given by:

$$\boldsymbol{F_{mag}} = (\boldsymbol{m} \cdot \boldsymbol{\nabla})\boldsymbol{B} \tag{2-6}$$

where $\boldsymbol{m}$ is the dipole magnetic moment and $\boldsymbol{\nabla B}$ is the external magnetic field gradient. By using Eq. 2-2, we obtain the usual magnetic force expression used in this work:

$$\boldsymbol{F_{mag}} = V_f\,(\boldsymbol{M} \cdot \boldsymbol{\nabla})\boldsymbol{B} \tag{2-7}$$

where V_f is the volume of the magnetic content [13].

On the other hand, in order to obtain magnetic susceptibility data from magnetophoretic experiments, it is usual to assume that the magnetic induction $\boldsymbol{B}$ and the magnetic applied field $\boldsymbol{H}$ are just related by permeability in free space, neglecting the effect of the magnetization $\boldsymbol{M}$:

$$\boldsymbol{B} = \mu_0 \boldsymbol{H} \tag{2-8}$$

By combining Eq. 2-3 and Eq. 2-8 we obtain:

$$\boldsymbol{M} = \frac{\chi}{\mu_0}\boldsymbol{B} \tag{2-9}$$

Then Eq. 2-7 becomes:

$$\boldsymbol{F_{mag}} = V_f\,\frac{\chi}{\mu_0}(\boldsymbol{B} \cdot \boldsymbol{\nabla})\boldsymbol{B} \tag{2-10}$$

Additionally as the moving particle displaces a fluid volume, it is also usual to take into account the magnetic force exerted on the medium, which leads to:

$$\boldsymbol{F_{mag}} = -V_f\,\frac{\chi_m}{\mu_0}(\boldsymbol{B} \cdot \boldsymbol{\nabla})\boldsymbol{B} \tag{2-11}$$

with χ_m the susceptibility of the fluid medium, and the minus sign indicates that this force is opposed to $\mathbf{F_{mag}}$. Then, the usual expression for the net force on a magnetic particle exerted by a magnetic inhomogeneous field is expressed in terms of the difference in susceptibility between the particle and the fluid:

$$\boldsymbol{F_{mag-n}} = V_f \frac{\Delta\chi}{\mu_0}(\boldsymbol{B}\cdot\boldsymbol{\nabla})\boldsymbol{B} \qquad 2\text{-}12$$

with $\Delta\chi = \chi - \chi_m$.

Finally, by applying a mathematical identity[2] and the fact that there are no electric currents involved in the discussed setup, we obtain:

$$\boldsymbol{F_{mag-n}} = \Delta\chi V_f \boldsymbol{\nabla}\left(\frac{|\boldsymbol{B}|^2}{2\mu_0}\right) \qquad 2\text{-}13$$

which is the other usual form encountered in articles related to magnetophoresis [13, 14, 15]. It is commonly supposed that the inhomogeneous magnetic field varies only in one of the coordinate axes, then the magnitude of the force can be written as:

$$F_{mag-n} = \Delta\chi V_f \nabla\left(\frac{B^2}{2\mu_0}\right) \qquad 2\text{-}14$$

where the operator ∇ is the standard derivative in the selected direction and *B* is the magnitude of the magnetic field in that direction.

2.1.3 Microfluidics basics

A microfluidics is a device that deals with fluid flow in channels with at least one dimension between 1 mm to 1 μm. When at least one of the dimensions of the channel is less than 1 μm, it is called nanofluidics.

Among the main advantages of microfluidics are: small sample quantities needed, high portability, fast and reliable results, and easy fluid control is possible.

---

[2] $\boldsymbol{\nabla}(\boldsymbol{B}\cdot\boldsymbol{B}) = 2\boldsymbol{B}\times(\boldsymbol{\nabla}\times\boldsymbol{B}) + 2(\boldsymbol{B}\cdot\boldsymbol{\nabla})\boldsymbol{B}$, as there are no electric currents $\boldsymbol{\nabla}\times\boldsymbol{B} = 0$

Fluid flows are characterized by the Reynolds number, a dimensionless parameter defined as:

$$Re = \frac{U_{flow} L}{\nu} \quad 2\text{-}15$$

where U_{flow} is the average velocity of the flow, L is the characteristic or most relevant length scale and ν is the kinematic viscosity of the fluid (defined as the dynamic viscosity μ divided by the density of the fluid ρ). This parameter describes the ratio between inertial and viscous forces in a fluid. The characteristic length *L* in channels is the hydraulic diameter D_h defined by:

$$D_h = \frac{4A}{P} \quad 2\text{-}16$$

with *A* the channel's cross-sectional area and *P* the channel's wetted perimeter.

Dimensions in microfluidics are small, which means that the Reynolds number is usually low, typically much less than 2100. This means that in microfluidics the flow regime is commonly considered as laminar flow. In this case, most flow patterns are simple, and are even expected to closely follow the geometry of the microfluidic channel [16].

When a rigid sphere moves in a microchannel and the Reynolds number for it is very low, the Stokes drag force formula is used:

$$\boldsymbol{F_{drag}} = -6\pi\mu r\boldsymbol{U} \quad 2\text{-}17$$

where *r* is the radius of the sphere, μ is the viscosity of the fluid and $\boldsymbol{U}$ is the microparticle's velocity.

By using Eq. 2-16 and Eq. 2-12 (or Eq. 2-13), and considering steady-state (no acceleration, i.e., drag and magnetic forces balance) it is possible to obtain an estimate of the magnetic susceptibility of magnetic microparticles by measuring their magnetophoretic velocity.

2.1.4 Magnetophoretic trajectory observation

Video imaging based analysis of particles trajectory was proposed in [17] to determine the magnetic susceptibility of large numbers of individual particles. This study utilized particle tracking velocimetry (PTV) on videotaped sequences. PTV is a technique intended to analyze complex fluid fields by tracking individual seeds circulating with the fluid. This technique was

first proposed with this name in [18]. In [19] the PTV's most recent algorithm version at the time is used. As PTV function is to visualize the fluid, particles are not individualized through the sequence of frames, which is a drawback in the proposed technique.

In [19, 20, 21] an instrument named as cell tracking velocimetry (CTV) was proposed for allowing the determination of the velocity of labeled cells and paramagnetic particles simultaneously by using microscopic video imaging and a computer algorithm, in a well-characterized magnetic energy gradient. The CTV had the objective of providing better insights for the outcomes to be expected in the magnetic cell separation process. The CTV is based on PTV, mainly solving the problem of particle's identification through video frames. CTV has been also used to investigate magnetophoretic mobility changes produced in human blood cells by some infections [22].

In the context of drug delivery mediated by the use of treatment vectors with embedded magnetic particles, an optical method to measure the magnetic response, in some way a simplified CTV setup, is proposed in [23]. The main differences with the CTV technique are a reduced setup size, and the use of a commercial program for particle tracking and video acquisition (CTV used videotaped sequences).

Recently a method called magnetophoretic trajectory tracking magnetometry (MTTM) has been presented [24] with the aim of measuring a quantity defined as relative specific magnetic susceptibility by fitting the particle's observed trajectories with theoretical curves. The main difference of this method with CTV is the fact that particle's recorded trajectories are long compared with particle size.

All techniques presented hitherto study magnetic particles or cells in a still fluid. A technique referred as magnetophoretic velocimetry was proposed in [25, 26, 27, 28] to determine paramagnetic species adsorbed by single droplets through the analysis of the acquired magnetophoretic velocity under a high gradient magnetic field. The magnetic susceptibility of the droplets was expected to change according to the adsorption and be reflected by a change in their magnetophoretic velocity. In this technique the capillary contains a fluid that is moving and the migration of species is observed as a deviation from the fluid flow acquired speed.

Magnetophoretic velocity measurements were also exploited to evaluate the particle uptake in magnetic labeling of cells [29, 30, 31]; in [7] the measured magnetophoretic velocity of magnetically coated microspheres roughly scaled with the surface area.

2.2 Magnetic Manipulation

Basic magnetic manipulation of particles in microfluidics is classified, according to Gijs [32], in:

- Retention and separation: usually magnetic particles are immobilized by using a magnet, the magnetic material is separated from the solution in this way and can be analyzed a posteriori. Several other alternatives exist, for example continuous flow separation by Pamme's group [39].
- Magnetic transport: In this approach, instead of deflecting the particles' trajectory while moving with flow, magnetic particles move because of the action of magnetic actuation. This kind of manipulation is difficult due to the particles' usual reduced magnetic volume.
- Magnetic labeling for detection: In this case, a magnetic label is attached to an entity of interest, and then detection devices are used to measure the produced magnetic field.
- Bead-flow interaction and mixing: magnetic particles tend to form chain-like aggregates due to dipole-dipole interactions. These aggregates can be used as plugs in certain applications, and by dynamically manipulating magnetic aggregations fluid mixing is possible in others.

One possible application of magnetophoresis is magnetic manipulation of magnetic particles as in separation, sorting and capture [15, 33]. For example, high gradient magnetic separation (HGMS) systems are used [34, 35, 36] to remove magnetic particles from a fluid flow. HGMS consists basically of a matrix of ferromagnetic material (wires or filaments) that captures magnetic particles as fluid flow passes through it while a high magnetic field is applied. After filtration has finished, the magnetic material is washed out as the magnetic field is turned off. The advantage of HGMS, to previous techniques of magnetic separation, is that allowed the trapping of relatively weak magnetic particles, which makes it suitable for biological applications [15].

As described in [37, 38], the relationship between magnetic manipulation and microfluidics is relatively recent. Pamme's group has developed a technique called free-flow magnetophoresis, a form of continuous flow separation that uses magnetic force to deflect the entities of interest [39, 40, 41, 42]. In this technique, magnetic particles are decoupled and deviated from their initial movement in a specific region of a magnetophoretic chamber. By these means, magnetic labeled particles exit the chip at specific positions depending on their magnetic properties. These outputs, with magnetic particles separated and sorted, can be used as inputs for other stages in more complex microfluidics applications. It is a continuous flow technique because magnetic particles are not trapped at certain regions of the microfluidics as in most other retention-separation methods. On the other hand, Furlani's group has focused in developing models for predicting magnetic separation in different microfluidics systems and applications [43, 44, 45, 46].

In [47] a microfluidic device was designed for magnetic bead immunoassays. The main focus in this work is to automate as much as possible the assay by incubating the microparticles in the reagent while in continuous flow. The microparticles are moved from sample flow to reagent flow by using a magnetic translational force.

Examples as the above ones show the potential use of the magnetophoresis jointly with microfluidics to manipulate magnetic or magnetically functionalized particles.

2.3 Magnetic Resonance Navigation

The concept of MRN (Magnetic Resonance Navigation) is defined in [48] and it can be summarized as a method in which magnetically loaded therapeutic/diagnosis microcarriers are propelled and navigated by using gradient magnetic fields while inside the bore of an MRI scanner. In the first attempts to use MRN, the gradient magnetic forces were produced by the standard imaging coils of a MRI scanner. Since these initial experiences with MRN using millimetric sized cores as proof of concept [3, 49, 50], it was clear that magnetic propulsion forces produced by imaging coils of a standard MRI scanner were not suitable to navigate micro/nano sized carriers. In [51] it was shown that to perform navigation of micron sized agents in the form of a suspension, the use of enhanced magnetic gradient coils is needed and it was clear that the magnetic aggregation between particles due to dipole-dipole interaction could influence targeting efficiency. In [6, 52] aggregations were studied more deeply and it was

suggested that, due to its increased magnetic volume, they could be used to compensate the reduction of the propulsion force acting on individual magnetic particles.

The potential use of magnetic aggregation to improve therapeutic effectiveness has been pondered by research groups that intend to use MRN for other applications. The use of MRN for lung treatment by using aerosol drug delivery was explored in [53]; they conclude that the use of magnetic agglomerations is needed in order to allow the navigation of magnetic loaded aerosol drugs in the lungs. The size of the agents used in lung treatment means that enhanced gradient coils, as those proposed in [51], are not able to generate the forces needed to steer the magnetic agents. Then, the only way to overcome this problem is by exploiting magnetic agglomerations. In other studies, they proposed a detailed mathematical model [54, 55] for the forces involved in the magnetic aggregation process. The expected advantage of this theoretical framework is the possibility for assessing the steering efficiency without the need of performing actual experiments. They compared simulation results with the experiences performed in [6], and they argued that the simulation framework agreed with experiences. However they get 100% efficiency in the same situation as the experiences, but in the experimental setup it was not observed. On the other hand due to the non-slip boundary condition, they expected 0% efficiency when needle-like aggregations were parallel to the main flow, which seems unlikely.

Another possible application for MRN is the cell transplantation therapy. In [56] it was shown that MRN could be suitable for cell transplantation therapies, and in [57] the effect of magnetic cell aggregation was studied as an important factor to increase targeting efficiency. The improvement in targeting efficiency was attributed to the fact that cell aggregations show a higher magnetophoretic velocity.

In the context of MRN, all the presented works concluded that the steering ratio could be enhanced by exploiting magnetic aggregation. On the other hand, therapeutic agents are expected to be synthesized in several ways depending on their expected usage. For example, some could contain higher quantities of embedded magnetic nanoparticles while other could contain more therapeutic drug. This diversity is expected to play a role also in the therapeutic agents' response to the exerted magnetic force produced by the gradient coils. For example, in [7] it was found that magnetic microspheres of the same size, prepared under similar conditions, presented magnetophoretic velocities differing by up to a factor of 4. Each one of the different therapeutic

agents could produce magnetic aggregations differing in size, stiffness, geometry, etc., and, therefore, behave differently in similar flow conditions and under the influence of the same magnetic gradient field. Moreover, in real treatment circumstances, physiological parameters could change unexpectedly. Additionally, in MRN fluid flow velocities are the ones found in human vascularity, which are relatively high when compared with fluid flow in experimental conditions in other applications.

To the best of our knowledge, there have been no other attempts to experimentally measure the trajectory of magnetic microcarriers in the context of MRN. In CTV and similar studies, there was no fluid flow involved; vertical and horizontal movements are due to gravity and magnetic force, respectively. The magnetic gradient was usually produced by a magnetic dipole, while in MRN it is produced by enhanced magnetic gradient coils. Finally, in our experimental conditions the magnetic micro-entities are inside the bore of a MRI scanner, therefore they are magnetized by the MRI's magnetic homogeneous field, and there are dipole-dipole interactions between them. All of these conditions justify the design of a magnetophoretic testbench to study the trajectories of magnetic microcarriers to be used for MRN treatments in order to quantify their response to a given magnetic gradient in terms of their deflection patterns.

2.4 Object tracking

Observation of magnetic microcarriers' trajectory means that software for their detection and tracking is needed. Object tracking has been the subject of a large amount of studies in computer vision and image processing [58] and has applications in many different areas as biology [59] and video surveillance [60]. The tracking problem can be defined as the survey of the movement that an object (or objects) follows in a sequence of frames of a video.

The first question to answer in this kind of application is to define the object to track. The answer to this question constitutes the way in which the object of interest is to be detected and represented. According to [58], the main object detection mechanisms are point detectors, background subtraction, segmentation, and supervised learning. In point detectors the aim is to find points in the object that are invariant to changes in illumination and camera viewpoint. Background subtraction uses a model for the static background and moving objects are frame regions that differ from this stationary background model (pixels that deviate from the

background model are marked for processing and are labeled as foreground pixels). Segmentation divides the image in partitions with similar characteristics. Finally, in supervised learning a training set is used to provide a model of the object to be detected. Once the object has been detected there are many ways of representing it, for example using geometric shapes, contours, points, etc. Usually this depends on the characteristics of the object being tracked. For example, for using in confocal microscopy, recently a new method for particle detection has been presented in [61] by exploiting radial symmetry of particles about its center. Particles' centers are located and represented as points. The algorithm determines the point of maximal radial symmetry by calculating the intensity gradient that it is expected to point towards the origins (particles' centers).

The next step in object tracking is to define the way in which the features selected representing the object are going to be located in the next frame given its position in the previous one. In this case, a displacement model is needed in order to define a search area. Some popular models used are deterministic translational model [62] and Kalman filter method that uses the state space approach. It is intended to deal with noise and random perturbations that usually occur in real video data [58].

Finally, once the search area has been determined, it is needed to locate the object in it and a matching criterion is needed. One of the most common matching criteria is template matching in which a representative instance (template) of the object is defined in previous frames, then this template is compared within defined search regions in the current frame by evaluating similarity functions. This approach is usually a brute force method, exhaustive in nature. Another common matching criterion is the brightness constancy used in optical flow that is based in the assumption that corresponding pixels in consecutive frames have no brightness change [58].

As pointed out in [59], it seems that automatic tracking results are still rarely perfect and experimental conditions usually produce problems to tracking tools in most of the cases, due to the fact that these applications are usually tightly linked to their specific application.

2.4.1 Particle Tracking

Object tracking applied to motion of particles uses several specific approaches and the literature on the subject is extensive. Only some algorithms used in particle tracking that are of interest for this project are presented here.

Micro Particle Image Velocimetry (μPIV): this technique is an adaptation of the Particle Image Velocimetry (PIV) technique for use in microfluidics. It was introduced by Santiago *et al* [63]. PIV techniques are intended to measure instantaneous fluid velocities. Usually fluorescent particles are seeded into the fluid flow and the particles' displacement is evaluated by image treatment techniques.

The typical PIV algorithm uses correlation to evaluate particles' displacement. Frames are divided into areas; these areas are called interrogation areas or windows. Mathematical correlation calculation gives a measurement of similarity between interrogation windows. The Fast Fourier Transform (FFT) is often used to obtain the correlation, then the peak location is estimated and the displacement is derived.

Correlation is usually calculated by using cross-correlation, but auto-correlation has also been used. In auto-correlation one frame contains a double exposure recording. The drawback with auto-correlation is that flow direction must be known prior to apply it, because it results in more than one correlation peaks (typically three). In cross-correlation method, each exposure corresponds to an individual frame, the correlation calculation results in a single correlation peak that contains velocity information [64].

Particle Tracking Velocimetry (PTV): the aim of this method is mainly the one of the PIV. The main difference is that in this technique few particles are tracked, compared with high particle densities used in PIV. In fact, is often called low-image-density PIV.

In PTV, seeded particles are identified and tracked in the frame sequence. As mentioned before, one of the first introductions of PTV is done in [18]. A typical PTV algorithm consists of two main steps: particle identification to locate particles in a given frame and matching algorithm to evaluate the position of the identified particle at different times. Most of the research effort for this method has focused on improving the matching feature algorithm used to track particles in frame sequences.

Some of the best known PTV matching methods are: nearest-neighbor search with geometrical constraints, cross correlation between two frames, relaxation methods that analyze the probability of particle matching and genetic algorithms [65].

Computer vision designed techniques have been adapted for PTV. For example, Ruhnau *et al*. [65] use optical flow to track particles, and recently in [66] a computer vision based approach has been proposed to deal with particles' overlapping problem in frame sequences.

Cell Tracking Velocimetry (CTV): this technique is a modified version of the PTV method used and developed in the Ohio State University [19]. This technique uses an image enhancement step prior to identification and tracking stages. The image enhancement steps are: histogramming used to find the range of the gray level present in the image, stretching used to improve contrast between particles and background, low-pass spatial filtering to remove noise, background subtraction and a final filtering step based on patterns to reconstruct incomplete cell images.

After image enhancement, the cell tracking algorithm is applied. This algorithm has two steps. The first step is cell location, which is based on a threshold level comparison to deduce if a given pixel is part of a particle (higher intensity than the threshold) or not. Once particles are located, a tracking module is used to establish the most probable path by using a sequence of five frames. The concept of path coherence is used to determine the particles' paths. This concept supposes that object trajectory should be smooth. In Figure 2-1 the method is shown; cells positions for each of the five consecutive frames are t_1, t_2, t_3, t_4 and t_5. Using the cell position in the first frame (t_1) as center, a search area is determined by radius "r" in the second frame. The determination of this radius depends on several considerations, usually ranges between 1 to 3 times the cell diameter. Once the position in the second frame (t_2) is established, the direction of movement and distance between them can be established (red line). From this information the location of the cell in the next frame is predicted (cell tagged as "p" near to t_3 in this example). The error between real and predicted locations is used in a penalty function used to determine path coherence; the smaller the value of the penalty function, the greater the path coherence. The penalty function is used when more than one cell is identified in the search area of the next frame; the path with the smallest penalty function value is selected as the correct path. The procedure is repeated for frames 4 and 5. Finally the process is reversed, that is, the analysis is

done starting with frame 5 and ending with frame 1. If penalty function values have large differences in forward and reverse directions, then the paths are defined as not reliable [67].

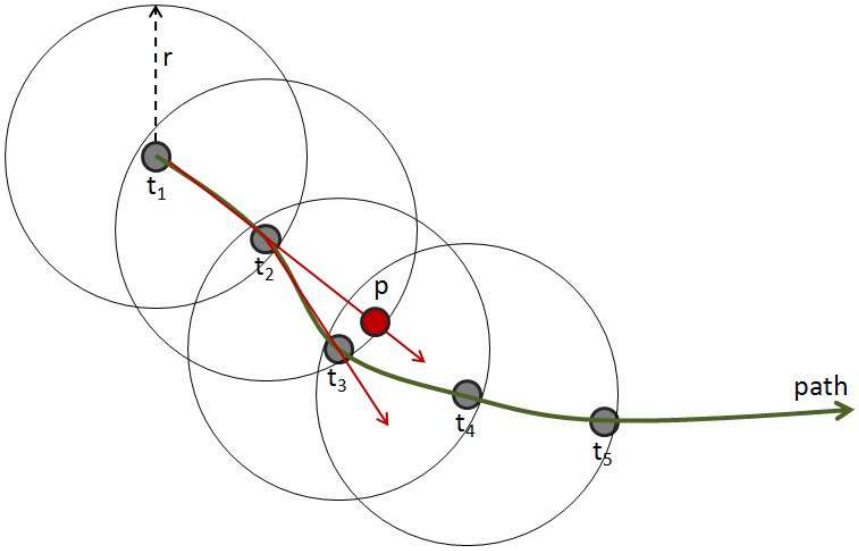

Figure 2-1 CTV method schematics. Cells identified in the five consecutive frames are named t_1 to t_5 respectively. The search area between frames is determined by radius *r*. A predicted location of the cell in frame 3 is indicated as *p*. The real cell path is depicted in green.

A multiple-frame PTV approach has been recently presented [68]. The main modification focuses in the way in which the prediction of particle position and velocity estimate is used to determine the radius of the search area in the next frame. It is expected that this method would improve the robustness and accuracy of PTV for highly seeded flows.

To summarize, to our best knowledge, the techniques to track moving particles have been adapted from methods used to study fluid flow behavior. PIV technique is commonly intended to provide information on the average fluid flow velocity, and PTV technique identifies and tracks individual particles. Given a specific problem, particle tracking approaches have been developed tailored to the specificities of the experimental conditions.

CHAPTER 3 OVERVIEW OF THE APPROACH

The aim of this thesis is to design a testbench device to characterize the microcarriers to be used as therapeutic/diagnosis carriers in order to better predict targeting efficiency in MRN treatments. The general goal of the MR-Sub project is to develop a navigation method for medical microcarriers to target deep regions in the human body by using an upgraded MRI system. This method has been demonstrated in vitro and in vivo [3, 4, 51].

In his Ph.D. thesis, J.B. Mathieu investigated the methods for navigating several microparticles as carriers for cancer treatment [69], concluding that magnetic aggregation of microparticles modifies their response significantly, but they were not completely characterized. The current work tries to build an incremental step in this subject by following some of the suggestions in J.B. Mathieu's work, focusing on the study of the deflection trajectories, i.e., magnetophoretic velocities of aggregations to allow a better treatment prediction.

In order to do so, first of all it was needed to develop a microfluidic device allowing measurements of magnetophoretic response of magnetic particles and aggregations. As exposed in the literature review, magnetophoresis has been used for sorting and separation purposes, then a microfluidic chamber inspired in these applications was designed and tested to record microparticle aggregation movements. This design was presented as a conference paper in [70]. This work is a proof of concept of the magnetophoretic chamber.

After having been able to record and estimate the magnetophoretic velocity of microparticle aggregations by hand, the paper presented in the next chapter addresses the problem of automatic data gathering. The main focus of the paper is to cover initial results using the sample application called blobtrack [71] from OpenCV for tracking of microparticle aggregations. The idea with this work is to explore improvements to the device and protocol designed and tested in [70]; and to provide the start point for the design of tracking software tailored for characterization of microcarriers intended to be used in MRN.

3.1 Microfluidic design

In order to understand the importance of the magnetophoretic velocity in the MRN it is necessary to return to physical features that make MRN possible. These physical features will guide the design decisions used to fabricate the microfluidics magnetophoretic chamber.

A general procedure in MRN can be summarized as follows: magnetic microcarriers are released in some predetermined point of the human vascular network (by using a catheter), then microcarriers are magnetically navigated through vessel bifurcations to reach the target location. The navigation is done following a predefined path. A schematic representation of a MRN procedure is shown in Figure 3-1.

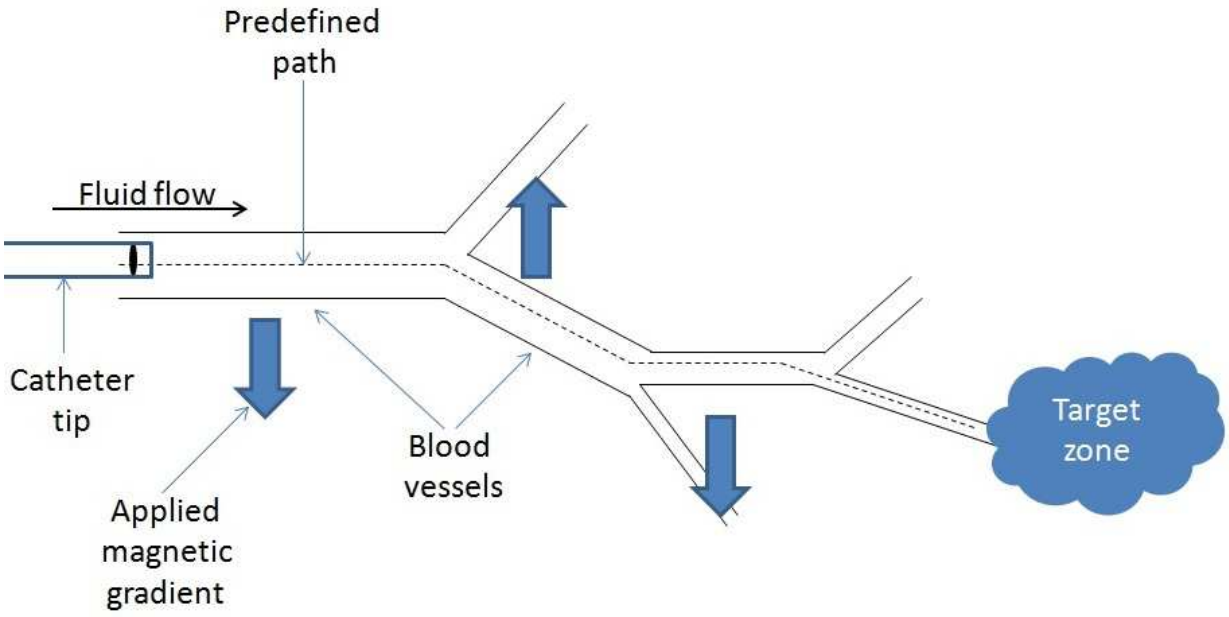

Figure 3-1 Schematic diagram of a general MRN procedure.

3.1.1 Relevant physics principles

As has been discussed in the precedent section, the action force used in MRN is due to a controlled magnetic spatial variation and is given by (Eq. 2-7):

$$\boldsymbol{F_{mag}} = V_f\,(\boldsymbol{M}\cdot\boldsymbol{\nabla})\boldsymbol{B} \qquad 3\text{-}1$$

with $\boldsymbol{M}$ (A/m) the magnetization, and V_f (m^3) the volume of the microcarrier's magnetic content; $\boldsymbol{\nabla B}$ (T/m) is the magnetic gradient applied. Inside the bore of the MRI scanner there is a constant field denoted B_0, usually big enough (1.5 T in the case of this project) to produce values close to saturation magnetization in the microcarrier's magnetic content.

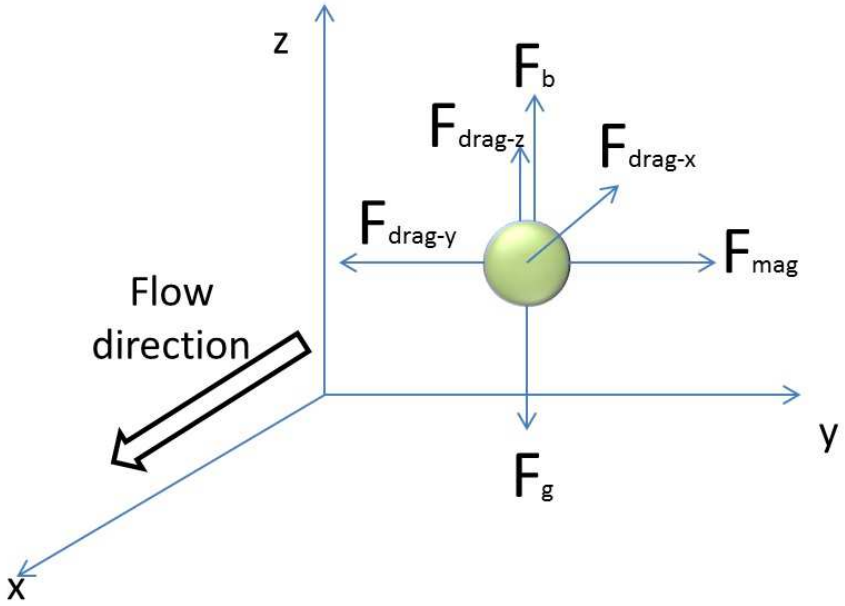

Figure 3-2 Free body diagram. Forces on a magnetic particle (green sphere in the center) in the magnetophoretic chamber are depicted. The fluid flow is in *x* direction. Magnetic force is applied in *y* direction. In *z* direction acts gravity and buoyancy. Drag force resist movement in all directions.

Figure 3-2 gives a general outline of the involved forces when a microparticle is moving in fluid flow. By applying the Newton's second law of motion we obtain that:

$$m\boldsymbol{a} = \boldsymbol{F_{mag}} + \boldsymbol{F_{drag}} + \boldsymbol{F_g} + \boldsymbol{F_b} \qquad 3\text{-}2$$

where m is the mass of the particle and **a** the acceleration, $\boldsymbol{F_{mag}}$ is the magnetic force applied in the *y* axis, $\boldsymbol{F_{drag}}$ is composed by $\boldsymbol{F_{drag\text{-}x}}$, $\boldsymbol{F_{drag\text{-}y}}$ and $\boldsymbol{F_{drag\text{-}z}}$ indicating fluid resistance to movement in all directions, finally $\boldsymbol{F_g}$ is gravitational force and $\boldsymbol{F_b}$ is buoyancy. In the context of this work, magnetic microparticles are supposed moving at the same speed of the fluid flow in the *x* axis, and then we consider that $\boldsymbol{F_{drag\text{-}x}}$ is zero. On the other hand, movement along the *z* axis is usually neglected. The net effect of this movement in the *z* axis is sedimentation (when the density of the

magnetic microparticle is large). Sedimentation is important because it causes the magnetic microparticles to touch the surface of the walls of the magnetophoretic chamber, and in that case, friction must be considered in the motion equation. The new simplified motion equation along the *y* axis is then:

$$m\boldsymbol{a} = \boldsymbol{F_{mag}} + \boldsymbol{F_{drag-y}} \quad 3\text{-}3$$

By using the simplifications exposed above, the only involved forces are the magnetic and the drag force along the *y* axis. Moreover, when particles are moving in a fluid, an equilibrium state is reached such that the net force is zero (acceleration becomes zero).

$$0 = \boldsymbol{F_{mag}} + \boldsymbol{F_{drag-y}} \quad 3\text{-}4$$

When the Reynolds number is very low (much less than 1), we have mentioned that the drag force $\boldsymbol{F_{drag\text{-}y}}$ is given by Stokes' drag force formula (Eq. 2-17). At equilibrium the magnetophoretic velocity is given by the balance between drag and magnetic forces, leading to:

$$\boldsymbol{F_{mag}} = \boldsymbol{F_{drag-y}} = 6\pi\mu r\boldsymbol{U} = V_f\,(\boldsymbol{M}\cdot\boldsymbol{\nabla})\boldsymbol{B} \quad 3\text{-}5$$

with μ the viscosity of the fluid, *r* the particle's radius and **U** the speed of the particle with respect to the fluid flow. The volume of the magnetic content V_f is related to the particle's radius *r* by:

$$V_f = \frac{4}{3}\pi r^3 \quad 3\text{-}6$$

By solving Eq. 3-5 for speed and using Eq. 3-6, the particle's magnetophoretic velocity is then given by:

$$\boldsymbol{U_{mag}} = \frac{2r^2(\boldsymbol{M}\cdot\boldsymbol{\nabla})\boldsymbol{B}}{9\mu} \quad 3\text{-}7$$

From Eq. 3-7 is clear that this magnetophoretic velocity can be adjusted by changing the size of the magnetic microcarrier (r^2 term), by altering the magnetic gradient ($\boldsymbol{\nabla B}$) or by adjusting the magnetic magnetization ($\boldsymbol{M}$) of the magnetic microcarrier.

This magnetophoretic velocity is a terminal steady velocity. It is important then to study the acceleration of the magnetic microcarrier as it approaches the steady-state to understand when it is possible to consider that the microcarrier has constant magnetophoretic velocity.

By using simplified relations in Eq. 3-5 and writing Eq. 3-3 in terms of the velocity we obtain the following expression:

$$m\frac{d\boldsymbol{v}}{dt} = V_f\,(\boldsymbol{M}\cdot\boldsymbol{\nabla})\boldsymbol{B} - 6\pi\mu r\boldsymbol{v} \qquad 3\text{-}8$$

assuming the magnetic force is applied only in the *y* direction, the solution to this equation is:

$$v(t) = \frac{V_f\,M\,\nabla B}{6\pi\mu r}\left(1 - e^{\frac{6\pi\mu r}{m}t}\right) \qquad 3\text{-}9$$

in which ∇ is the derivative in the *y* axis; and *M* and *B* are the magnitudes of the magnetization and the inhomogeneous magnetic field.

From Eq. 3-9, the characteristic time scale in this situation is:

$$T = \frac{m}{6\pi\mu r} \qquad 3\text{-}10$$

This characteristic time scale has been usually considered very small [16]. The assumption that the magnetophoretic velocity is the one given by Eq. 3-7 is safe in that case. However, when magnetic particle aggregations are being investigated, the size of the new "equivalent" microcarrier could increase the relaxation time due to Eq. 3-10 dependence on the mass of the new magnetic microcarriers aggregation.

3.1.2 Biological considerations

Blood flow velocity is usually very high in human vasculature. Common medium arteries in human are 2 mm to 6 mm in diameter, and flow velocities can range from 10 cm/s to 60 cm/s [72, 73, 74]. Figure 3-3 shows typical sizes and blood flow velocities in the human vascular system. In his work, Pouponneau *et al.* [5] used a bifurcation with a width of 2.5 mm to model a hepatic rabbit artery to test the feasibility of different ways to produce TMMCs to target liver cancer. In this work, it is also stated that the minimum size for microparticles used in liver embolization (in terms of their diameter) is 40 µm.

Due to the fact that Eq. 3-10 indicates that the relaxation time for this kind of experiments can be usually considered negligible, the magnetic microparticles and magnetic aggregations inside the magnetophoretic chamber are considered moving with the terminal magnetophoretic velocity when the magnetic gradient is applied.

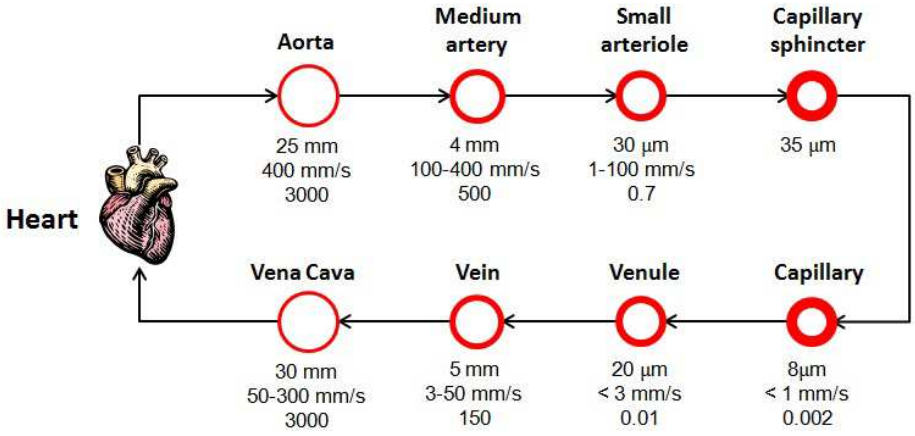

Figure 3-3 Schematic representation of human cardiovascular system vessels. Vessels' main parameters depicted are inner diameter, average blood flow speed and Reynolds number adapted from [72].

Based on the above information, the magnetophoretic chamber was designed to be 6 mm wide in order to simulate most of the distances that magnetic microcarriers are expected to cross. Plexiglas (PMMA) was selected as the material for fabricating the magnetophoretic chamber. Among its advantages one can mention low cost and high transparency (vital for magnetophoretic experiences) [75].

In MRN treatments, magnetic microcarriers are normally being injected in a vessel close to the targeted area by using a catheter. In [4] a catheter with a lumen[3] of 0.7 mm (700 µm) is used to perform the experiments. This diameter was selected because it did not cause the magnetic microparticles aggregations to clog when the injection was performed. This information is used to decide the size of the channel that transports the magnetic microparticles into the magnetophoretic chamber. In order to allow similar conditions as the ones expected in real MRN experiences, the width of the entrance channel is selected as 500 µm.

In the same study [4], the designed TMMC particles are released between 20 and 30 mm from the bifurcation. In [76] the injection point in simulations is situated at 15 mm from the

[3] Lumen: size of the inside space of the tubular structure of the catheter.

bifurcation. This data is used to estimate that the magnetophoretic chamber should be about 15 to 20 mm long in order to emulate previously used experimental conditions.

As has been mentioned above, blood flow speeds for the sizes considered are quite large (between 10 cm/s to 60 cm/s). For a typical blood flow of 15 cm/s, the time to travel the expected 15 mm long chamber would be 10 ms. For a frame rate of 15 frames/s (which is the typical rate obtained with the MRI compatible camera), one frame is taken every 66 ms; then one could not be able to record the movement. In order to obtain 15 frames to analyze the deflection movement of a magnetic particle or a magnetic aggregation, 1500 frames/s would be needed. The video output signals of the MRI compatible camera are NTSC or PAL video signals, which gives a maximum of 30 frames/s (for NTSC). With this in mind, in order to obtain several frames to analyze deflection patterns, fluid flow speed must be reduced. Then in order to obtain at least 7 frames to analyze, the fluid flow should be no more than 30 mm/s.

3.1.3 Chamber

The initial chamber design was inspired by Pamme's design used for continuous fluid flow separation [39]. In this design the magnetophoretic chamber is 6 mm by 6 mm with 16 plus 1 inlets of 100 µm wide evenly spaced and 16 outlets of 100 µm wide evenly spaced also, designed as a tree like succession of bifurcations. The chip is fabricated in glass, and the flow is produced by a syringe pump in withdrawal mode connected in the output. As pointed out before, the injection point in previous experiences was placed at 15 mm or more from the point of interest (bifurcation in this case). Then the design was modified to fit with the size of interest in our application. The number of inputs and outputs was reduced from 16 to 8 (plus the extra one in the input side).

Because of the use of PMMA instead of glass and the chamber's aspect ratio, the chamber was not at all functional due to deformations in the middle of the channel. Even using the pillars described in Pamme's work [39], it was not possible to avoid this bending. In Figure 3-4 the deformation problem is schematically shown. Fluid flow moves in the *x* axis, the magnetic force is applied in the *y* axis and the deformation of the channel is in the *z* axis (not indicated). The resulting deformation in the *z* axis reduced the depth of the chamber in its center. In such a case, the fluid flow tended to move around the bending zone in the microfluidic chamber as depicted in

Figure 3-4. In addition, the negative pressure produced by the use of the syringe pump in withdrawal mode increased the bending effect in the center of the magnetophoretic chamber.

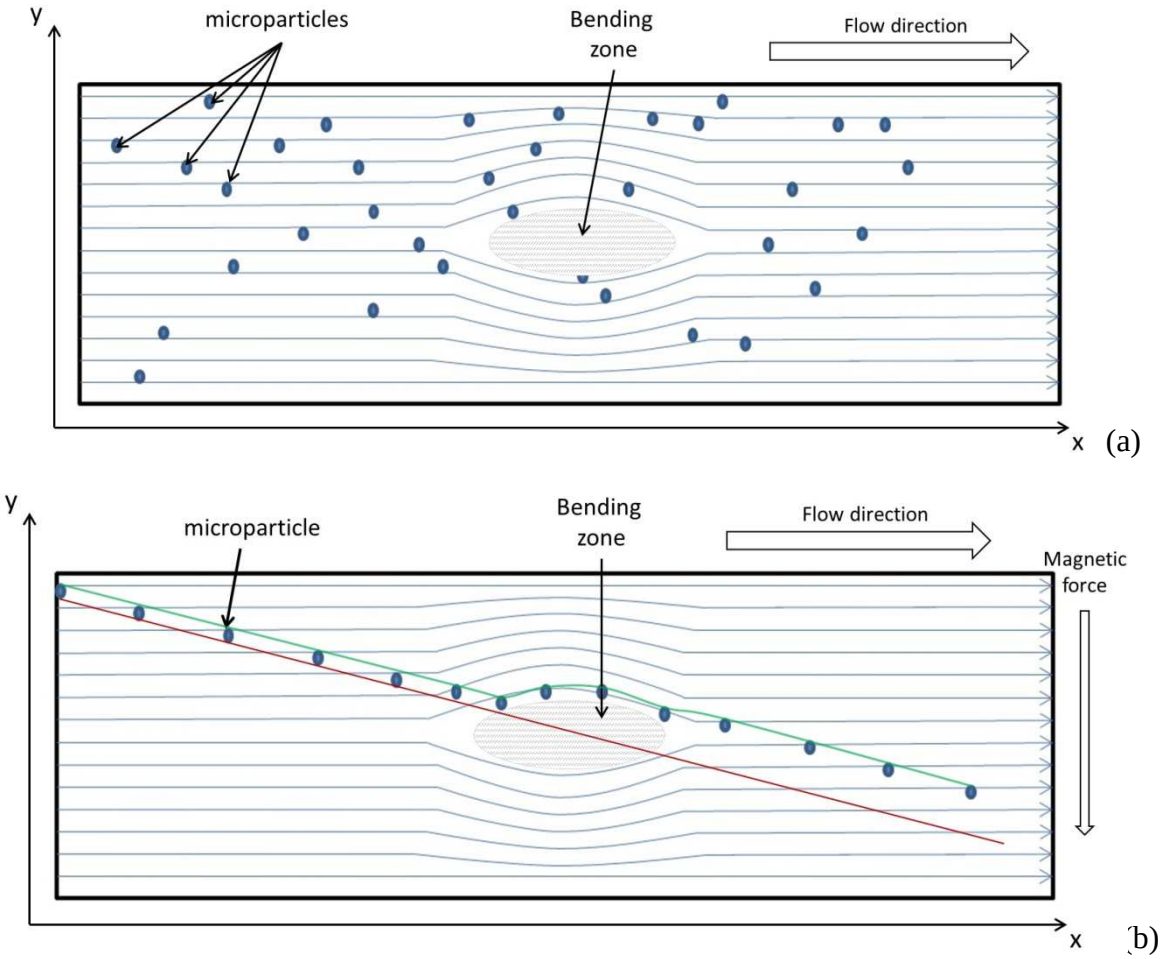

Figure 3-4 Bending problem in the initial chamber design. (a) Without magnetic steering force applied. Magnetic microparticles are represented in blue. Stream-lines are represented by blue arrows crossing the chamber. The bending zone is indicated in the middle of the chamber. (b) Expected effect on a magnetic aggregation when the magnetic force is applied. The expected deflection trajectory is shown in red; the effect of the bending zone on deflection pattern is shown in green.

Another difficulty found with this initial approach was the tree like design of the input and output channels. This design was supposed to evenly spread the fluid flow in the chamber. Initial

tests proved that this design decision was a problem in our case, mainly because of the air bubbles. In any symmetric bifurcation, any perturbation can destroy the symmetry of the flow. The air bubbles tended to clog the branches where they stay, avoiding the liquid to flow, and then perturbations were produced in the flow inside the chamber.

Based on these initial tests, the microfluidic design was modified to try to avoid as much as possible the problems found. The size of the magnetophoretic chamber area was reduced to 6 mm wide by 7 mm long. The microfluidic device is designed to measure and record microparticle trajectories, and not to collect them according to their magnetophoretic velocity. Accordingly, the input and output networks were transformed into single channels. The connection between input and output channels is performed in angle (Figure 3-5 (b)). The design is done taking into account that a right angle can produce turbulences in the fluid flow (Figure 3-5 (a)), and then the entrance and exit from the chamber are done in 45° in order to avoid this effect and obtain a smoother fluid flow (Figure 3-5 (b)).

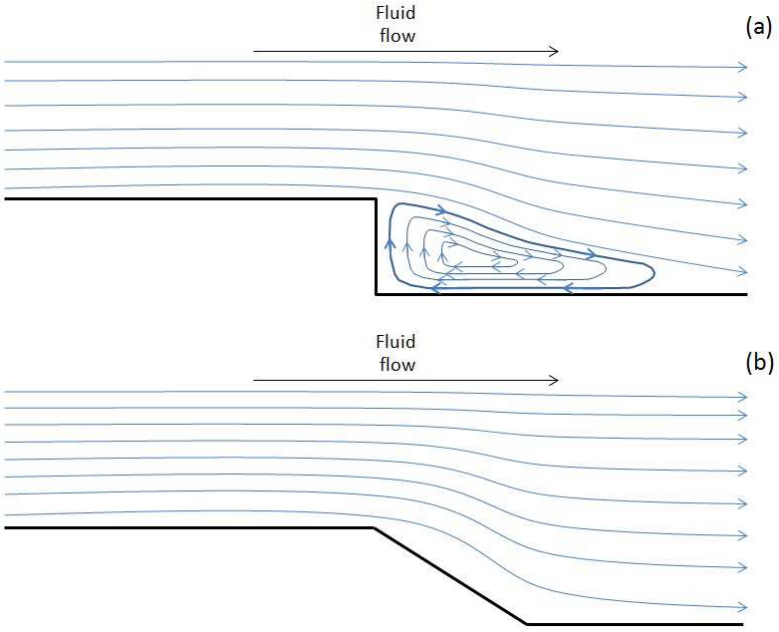

Figure 3-5 Schematics of fluid flow streamlines in channel connections. (a) Schematics of fluid flow streamlines for right angle channel connection with vortex roll forming at the entrance of the magnetophoretic chamber (adapted from [16]). (b) Schematic of smoothed fluid flow by using angle connection.

The input inlet for microparticles was moved to the center of the chamber in order to imitate the usual situation in the treatment where the catheter is expected to release the diagnosis or therapeutic magnetic microcarrier around the center of the selected vessel. The microparticles inlet is designed to be 500 µm in accordance with the inner diameter of catheters and to avoid clogging due to microparticle aggregations.

The main fluid channel is designed as a bifurcation to allow the use of one syringe pump to produce the main fluid flow. The microfluidic device can be used in negative (syringe pump connected at the exit of the microfluidics in withdrawal mode) or positive pressure (syringe pump connected in the main flow inlet in normal mode) regime. Due to the lessons learned during the tests of the initial chamber design, the syringe pump is used in normal mode to alleviate the bending in the center of the chamber.

In order to deal with the bending of the center of the chamber, various bonding techniques were tried. Bonding of PMMA plates is done using an oven, where the pressure and temperature can be controlled. The right balance between pressure and temperature allows the minimization of the deformation effect in the microfluidic device. The glass transition temperature for PMMA is around 105 ºC. At this temperature, PMMA starts to soften, if pressure is then applied to the PMMA substrates, they affix together. The problem is that as PMMA softens, the substrate can change its geometric properties during the bonding process.

The following PMMA bonding techniques were tried:

- Low pressure, high temperature bonding: a relatively high temperature of 165 ºC is used, and in order to avoid channel deformations, very low pressures are needed [77]. The results when using this technique were worse than what was obtained with the typical configuration of the oven usually used in the Nanorobotics Lab.
- Low temperature, high pressure bonding: the idea in this case is that the PMMA substrate is kept below the glass transition temperature 95 ºC which ensures its rigidity during bonding [75]. Again results when using this technique were worse than what was obtained with the typical configuration of the oven usually used in the Nanorobotics Lab.

- Thermal bonding in water: in this technique PMMA substrates are clamped together and immersed in boiling water during 1 hour [78]. The results were even worst with this technique. The PMMA plates were completely deformed during the process.

In the end, the bonding method used in this work was based on the previous settings of the oven with some slight variations in order to decrease the bonding temperature and pressures such that the geometry of the chamber was better maintained.

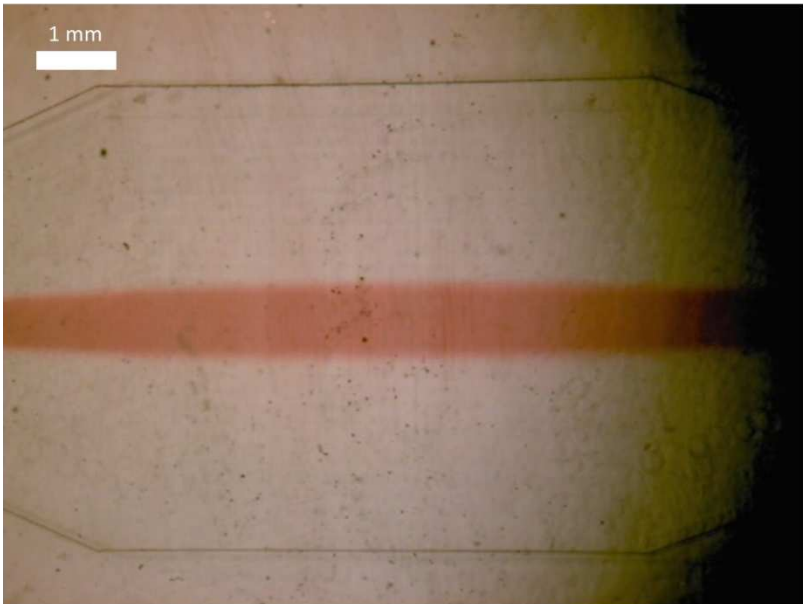

Figure 3-6 Flow pattern in the magnetophoretic chamber. Flow observed in the magnetophoretic chamber when ink is pumped in the microparticles inlet and DI water in the main flow inlet.

In order to verify that the chamber was going to direct particles to the center of the magnetophoretic chamber and to calibrate the relationship between syringe pump speeds, experiments were performed by injecting ink in the microparticles inlet, while DI water was pumped in the main flow inlet. Once calibrated, the observed flow pattern is shown in Figure 3-6, it can be noticed that ink flow goes straight forward to the outlet of the chamber. It can also be noticed that laminar flow has been achieved as the size of the ink flow has a relatively constant width, which indicates that no turbulences are observed.

3.2 Microparticles

As mentioned before, TMMC have been designed in our laboratory and have been already demonstrated [4]. The obvious choice for magnetic microparticles to try the magnetophoretic chamber was to use TMMC, however these were not available. These microparticles were produced in limited quantities to demonstrate that it is possible to produce magnetic loaded drug carriers for use in MRN tretaments. Then it was needed to select ones with similar characteristics to the TMMC used in [4]. TMMC have a mean diameter of 53 μm, are polydisperse and have a magnetization of 250 kA/m.

PS-MAG-S1986 microparticles from Microparticles GmbH (Berlin, Germany) were used in this project. These microparticles have a mean diameter of 41.13 μm, are monodisperse, and have a magnetization of 36 kA/m in a field of 1.5 T as typical found in clinical MRI scanners[4].

These microparticles exhibit a diameter almost equivalent to the TMMC that have been successfully navigated in the hepatic artery of rabbit models with controlled release of the therapeutic agent in specific locations in the liver [4]. Moreover, in [5] it is established that 40 μm is the minimum average diameter for embolization, then even if there are other commercially available magnetic microparticles with a magnetization values closer to the TMMC ones, their diameter was much lower than 40 μm, then PS-MAG-S1986 microparticles were preferred.

3.3 Simulations

Based on Eq. 3-3 and Eq. 3-8, a simulation framework was designed to evaluate the possible outcomes of the experiences using the magnetophoretic chamber described in the previous section. The simulations were done using Matlab.

The simulation is a very simplified version of Joerg Buchholz's Particle System Toolbox [9]. Basically time is divided into steps that are used to evaluate the acceleration in the *y* axis as expected from Eq. 3-8. Then velocity and position in the *y* and *x* axis are evaluated by using the following relationships:

---

[4] Monodisperse: particles have uniform size distribution. Polydisperse: particles have varied sizes distribution

$$v_{y-next} = v_{y-prev} + ac_{y-prev} * time_step \quad 3\text{-}11$$

$$y_{next} = y_{prev} + v_{y-prev} * time_step + \frac{1}{2} ac_{y-prev} * time_step^2 \quad 3\text{-}12$$

$$x_{next} = x_{prev} + v_x * time_step \quad 3\text{-}13$$

As can be seen, the velocity in the *x* axis is assumed to be constant because it corresponds to fluid flow acquired velocity. The simulation starts when the particle arrives at the magnetophoretic chamber, and so, the initial *y* axis velocity is assumed to be zero.

Simulation results were used to compare experimental findings with theoretical ones in a conference paper [70]. There is no study on the influence of the initial position in this simulation. Microparticles are supposed to be perfect spheres to evaluate the drag force. Possible existing friction forces and gravity have been neglected for the purpose of this initial screening of the expected results by using the magnetophoretic chamber.

Due to the reasons exposed before, 4 fluid flow speeds have been selected with a maximum of 20.8 mm/s. The other 3 fluid flow velocities were chosen to be successive speed halves (i.e., 10.4 mm/s, 5.2 mm/s and 2.6 mm/s). In this way it is expected to be able to study the effect of the fluid flow on deflection patterns of magnetic particles and magnetic aggregations when a magnetic gradient is applied.

Simulation results are shown in Figure 3-7. The low magnetization of the magnetic microparticles used could explain that it is not expected that they will be able to cover individually the 3 mm trajectory in the *y* axis for any of the flow velocities considered. The simulation parameters used in this simulation are shown in Table 3-1.

The resulting individual microparticle magnetophoretic velocities (measured as the distance reached in the *y* axis while 7mm have been reached in the *x* axis, divided by the time that this takes) are: 69 µm/s at a fluid flow of 20.8 mm/s; 153 µm/s at 10.4 mm/s; 304 µm/s at 5.2 mm/s and finally 534 µm/s at 2.6 mm/s.

If real human flow speeds are considered, it is not expected that individual microparticles are going to be able to travel the 3 mm distance in the y direction due to the action of the magnetic force. Initial simulation results show that if using the magnetic microparticles considered here, the blood flow should be slowed down (this has been done before using

catheters with a ballon on its end). However 3 mm is considered the worst case scenario. What is really needed is that the magnetic microcarriers should reach the fluid flow streamlines that are going to permit them to enter the expected bifurcation branch, then most of the distances that they have to traverse are much less than the worst case scenario.

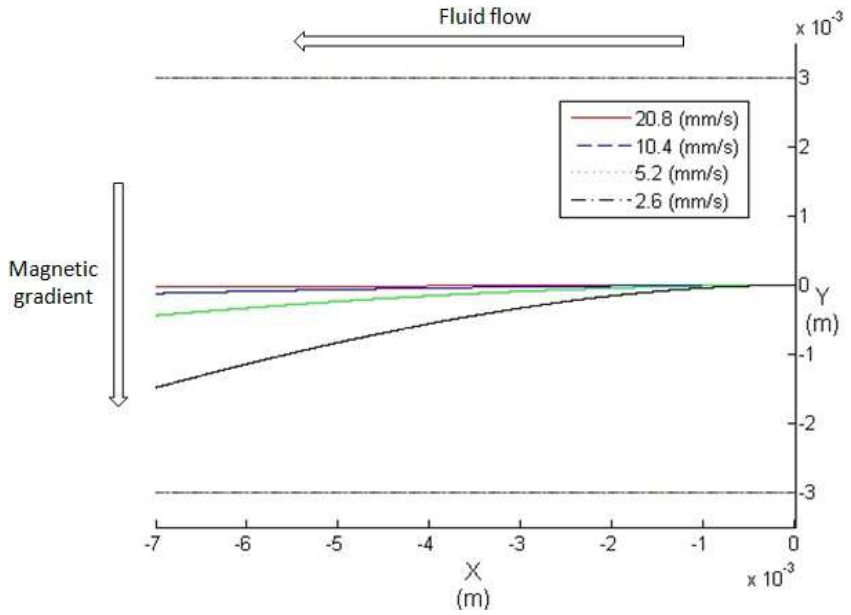

Figure 3-7 Simulated individual microparticle's deflection patterns. Flow velocities considered are 20.8, 10.4, 5.2 and 2.6 mm/s (from top to bottom in the graphic).

Table 3-1 Simulation parameters

Name	***Units***	***Value***
Microparticle diameter	m	41.13×10^{-6}
Microparticle mass	kg	9.035×10^{-7}
Microparticle magnetization	A/m	36×10^{3}
Magnetic gradient	T/m	0.4
Water viscocity	Pa·s	0.001

The next question to respond by simulation was the effect of magnetic aggregation on the trajectories of the magnetic microcarriers. According to [79], 280 magnetic microparticles can be safely used in the form of bolus injections allowing not blocking the tip of the catheter. The theoretical therapeutic treatment followed in this way would last around 30 minutes with the injection of about 380 of such boluses every 5 seconds approximately. In such case, the total mass using data inTable 3-1 would be 2.53×10^{-4} kg and an equivalent sphere with the same volume as 280 microparticles in chain like aggregation would be 308.0×10^{-6} m (the derivation of this diameter value can be found in the Appendix 1). The resulting expected trajectories for magnetic aggregations of 280 magnetic microparticles are shown in Figure 3-8.

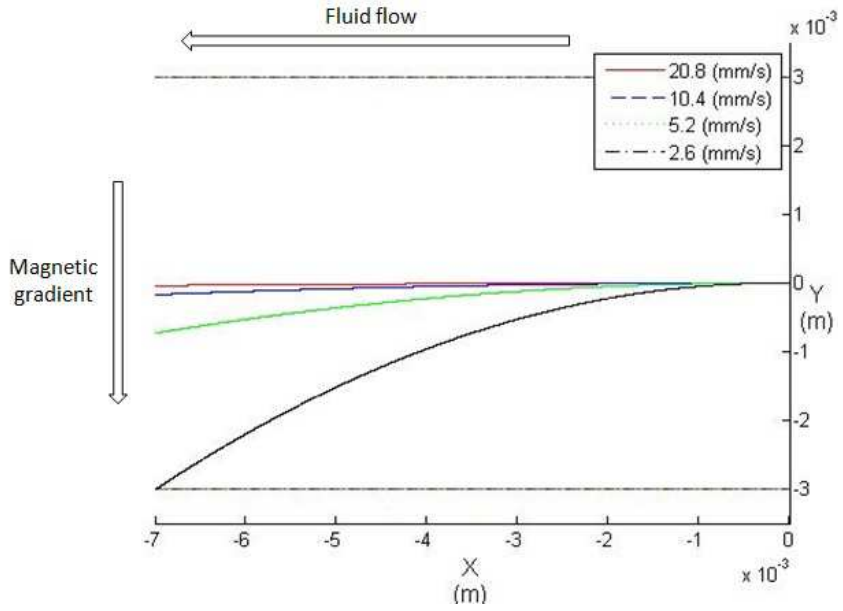

Figure 3-8 Simulated microparticles aggregations deflection patterns. Flow velocities considered are 20.8, 10.4, 5.2 and 2.6 mm/s (from top to bottom in the graphic).

The resulting final magnetophoretic velocities are: 107.34 µm/s at a fluid flow of 20.8 mm/s; 251.25 µm/s at 10.4 mm/s; 541.21 µm/s at 5.2 mm/s and 1.11 mm/s at 2.6 mm/s. In this case one should expect that magnetic aggregations of the size as the ones proposed in [79] should traverse the entire *y* axis of the chamber only in the case of the lowest fluid flow velocity.

3.4 Experiments

The experiments were designed to test the viability of the magnetophoretic chamber as the base for future developments to study the deflection behavior of magnetic microparticles subjected to a magnetic force. One of the main objectives of the experiences is to study magnetic microcarriers aggregation by evaluating their response to a magnetic gradient. From simulations shown before, it seems clear that, even if the size of the magnetic material is increased (by using dipole-dipole interaction between magnetic microparticles), the main obstacle to control magnetic microcarriers is the fluid flow speed in the human body.

3.4.1 General setup

The experimental setup consist of a PMMA phantom, designed following the process mentioned before, positioned in the center of a custom built Maxwell pair coil generating the magnetic gradients. The whole system is placed in the middle of the bore of a commercial MRI scanner providing the constant 1.5 T main magnetic field.

Two syringe pumps are used to control the main and magnetic microparticles fluid flows. Magnetic microparticles are introduced in the fluid flow by using a 3-way switch placed inside the MRI scanner bore. This way of injection was selected instead of pumping microparticles from outside the MRI scanner bore; because in the vicinity of the entrance to the MRI bore the magnetic field is not constant, then magnetic aggregations tend to move in an uncontrollable fashion. Moreover, syringe pumps must be placed around 2 m far away to avoid the magnetic force in the vicinity of the MRI bore act on them, then magnetic microparticles tend to sediment in the tubing before reaching the PMMA microfluidics. This procedure is based on the methodologies described by J.B. Mathieu in his thesis [69].

The Maxwell pair coil is able to produce 22.15 mT/m for each A, at 18.05 A produces approximately 400 mT/m. It has a rise time of 10 ms. Each coil has a diameter of 12 cm and the space between them is 10 cm. The Maxwell coil pair is driven by a KIKUSHI PBX 20-10 bipolar power supply manually controlled. The microfluidic device is oriented perpendicular to the main static field B_0 of the MRI scanner. The magnetic gradient generated by the Maxwell pair is oriented parallel to the main static field.

3.4.2 Experimental results

The initial experiences showed good agreement with the expected results for aggregations. At lower flow speeds (2.6 and 5.2 mm/s) simulation results seem to fit relatively well with experiments. Supposing rod-like aggregations as in Figure 3-8, for a flow speed of 5.2 mm/s the experimental magnetophoretic velocity was 44% faster than simulated one, and in the case of 2.6 mm/s experimental magnetophoretic velocity was 14% faster than simulation result. The results were presented in a conference paper in the International Conference on Manipulation, Manufacturing and Measurement on the Nanoscale (3M-NANO 2012). The deflection patterns were similar to the ones shown in Figure 3-8. As expected from simulations, the only case in which the aggregations were able to cover the 3 mm distance was for a fluid flow velocity of 2.6 mm/s.

The main problem with this initial setup is the fact that magnetic microparticles are relatively heavy, and then sedimentation cannot be safely neglected, which could explain differences with simulations. Another problem is the injection methodology, the control of aggregates dimensions and shapes is not the subject of this investigation, but a better controlled way to inject and produce magnetic microparticle aggregations could certainly be beneficial in magnetophoretic experiences.

Initial magnetophoretic velocities for magnetic aggregations were estimated as 0.95 mm/s in a fluid flow speed of 2.6 mm/s, 0.78 mm/s in a fluid flow speed of 5.2 mm/s, 0.90 mm/s in a fluid flow of 10.4 mm/s, and 0.92 mm/s in a fluid flow of 20.8 mm/s. These measurements were done by hand counting the number of frames and the total distance that the aggregations have travelled from the first frame magnetic force is applied through the end of its deflection trip. These results compare relatively well with simulation results shown for rod like aggregations, especially for the fluid flow speed of 2.6 mm/s where simulations indicate 1.11 mm/s and experimental results show 0.95 mm/s.

3.5 Tracking tool

After promising results from the magnetophoretic chamber, it was decided to investigate the feasibility of using a software tracking tool to integrate with the magnetophoretic chamber, then creating a complete magnetophoretic behavior testbench.

The paper presented in the following chapter shows the results of applying a modified version of the OpenCV blobtrack [71] sample application to track magnetic particle aggregations in the magnetophoretic chamber. This tracking tool was used in Peng's thesis [8] to track aggregations when using a fuzzy controller.

After these tests it was decided to develop a software tool specific for magnetophoretic experiments. The software tool is designed to present a solution to the goal of identify moving particles in digital videos taken from magnetophoretic experiences and to obtain the magnetophoretic velocity by following their movement, taking into account the specificities of the magnetophoretic experiences instead of using a general tracking tool as the blobtrack one. The initial step was to decide the adequate development platform and tools to develop it.

The tool is developed in C++ because it has the following advantages:

- it is a language that has good support for mathematical and graphics processing,
- it allows good modularity which allows better comprehension of the software and makes it easier to change, and
- it provides high and low level programming options.

In order to get the image processing tools, it was chosen to continue using OpenCV due to the following characteristics of it:

- as indicated before, there is some exposition to it in other projects, then this knowledge can be used in this project,
- it is a mature open source initiative (more than 10 years of development),
- it includes several image processing tools proven methods for object tracking,
- it is compatible with C++ programing language, in addition with Python support for rapid prototyping,
- it has an active internet community allowing easy access to support and examples, and
- it is a cross-platform tool (supports Windows, Linux, iOS and Android).

Finally in order to develop a GUI for the tracking software tool, Qt was selected due to:

- its integration with OpenCV,

- it is an open source framework,
- it provides a comprehensive set of tools for GUI development, and
- it is cross-platform.

CHAPTER 4 MEASURING THE MAGNETOPHORETIC CHARACTERISTICS OF MAGNETIC AGENTS FOR TARGETED DIAGNOSTIC OR THERAPEUTIC INTERVENTIONS IN THE VASCULAR NETWORK

4.1 Title Page

Measuring the magnetophoretic characteristics of magnetic agents for targeted diagnostic or therapeutic interventions in the vascular network

Guillermo Vidal, Sylvain Martel

NanoRobotics Laboratory, Department of Computer and Software Engineering,

École Polytechnique de Montréal (EPM) Montréal, Canada

Phone: (514) 340 4711 ext. 5098

Fax: (514) 340-5280

email: sylvain.martel@polymtl.ca

URL: http://wiki.polymtl.ca/nano/

Note The author acknowledges the financial contributions from the Canada Research Chair (CRC) in Micro/Nanosystem Development, Fabrication and Validation and grants from the National Sciences and Engineering Research Council of Canada (NSERC), the Province of Québec, and the Canada Foundation for Innovation (CFI). G.V. was financially supported by a CONICYT scholarship for M.A.Sc. studies and support abroad (BECAS CHILE).

Status: published online paper in **Journal of Micro-Bio Robotics**, February 1st 2013.

4.2 Abstract

An experimental setup for characterizing the magnetophoretic properties of magnetic therapeutic microcarriers and/or diagnostic agents is described. Such characterization is essential for determining the optimal sequences of magnetic gradients to deflect its trajectory through relatively complex vascular networks in order to reach a predetermined target. The recorded magnetophoretic data can be used to predict the path of the agents when submitted to directional gradient fields and under different fluid flow velocities. Automatic extraction of these data is performed using a tracking method.

4.3 Introduction

Minimally invasive cancer treatments have recently aroused much interest. Magnetic Resonance Navigation (MRN) is a technique aimed at navigating magnetic microcarriers [3, 50, 51] such as Therapeutic Magnetic Micro Carriers (TMMC) [4, 5] for drug delivery in cancer therapy. This drug delivery system promises improvements in therapeutic and diagnosis by increasing targeting efficacy while avoiding or at least minimizing systemic circulation often causing added toxicity in healthy organs.

The basis of this method consists in the use of the magnetic homogenous field and the magnetic gradients of an upgraded clinical Magnetic Resonance Imaging (MRI) scanner to magnetize the soft magnetic nanoparticles inside the microcarriers and to steer them respectively along a planned trajectory in the vasculature towards a targeted destination. This method has been validated in-vivo in [3, 4].

With a reduction of the size of the magnetic drug carriers to accommodate narrower blood vessels, the amount of therapeutics being delivered is reduced as well. To compensate, magnetic aggregations of MR-navigable therapeutic microcarriers are used. Such magnetic aggregations of microcarriers will be characterized with magnetophoretic velocities [6, 52] which differ from single microcarriers.

As a consequence, collecting reliable data such as with an optical method [23] on the magnetic responsiveness in term of deflection patterns of such magnetic microcarriers is critical for determining the optimal control sequences during MRN in order to achieve a higher Magnetic Resonance Targeting (MRT) efficacy with a given type of MRN-compatible agent during

targeted medical interventions. Indeed, several types of such therapeutic agents could be synthesized with various sizes, while embedding a larger quantity of magnetic nanoparticles to enhance responsiveness to magnetic gradients or with less magnetic nanoparticles to allow a higher density of therapeutics to be delivered. In turn, a higher or lower concentration of magnetic nanoparticles within each microcarrier will affect the dipole-dipole interactive forces among neighbored microcarriers which would have a profound impact on the overall magnetic response of the aggregates to specific magnetic gradients.

The importance of aggregation has been addressed in several works. In [53], Vartholomeos *et al*. argue that magnetic aggregation could be used to increase therapeutic effectiveness of aerosol drug delivery for lung treatment while in [57] Riegler *et al*. explore the aggregation of labeled cells for use in cell transplantation therapy. References [6, 52] suggest that magnetophoretic velocity of aggregations and the fraction of aggregated versus non-aggregated particles needs to be precisely estimated in order to get better targeting predictions prior to conduct MRN.

The goal of this study is to design and test a magnetophoretic testbench. The initial results with the testbench were presented in [70].

In order to build a useful tool for characterization of new therapeutic/diagnostic microcarriers, the testbench must include some sort of automatic tools. As has been discussed above, the range of variability between magnetic microcarriers can be very large. On the other hand, the statistical meaning of the measurements is governed by the capacity to manage a big enough amount of runs each time a new microagent is evaluated. As pointed out in [70], a major drawback of the current design is the need to synchronize the magnetic gradient with the entrance of particles in the magnetic chamber. It is also clear that, even if another chamber design solves this inconvenient, software for detection and tracking of the microparticles aggregations is needed. An initial evaluation of the feasibility of the detection and tracking is discussed here.

The testbench is experimentally tested by measuring the magnetophoretic velocity of MRN microcarriers relying on embedded nanoparticles in the bore of a clinical MRI scanner; and evaluating the effect of the flow rate on the deflection of these magnetic micro-entities. The results presented in [70] are used to evaluate the tracking method for data detection and acquisition.

4.4 Theoretical background

4.4.1 Particle movement

The magnetic propulsion force induced by a magnetic gradient ∇B on a magnetic particle or magnetic aggregation is:

$$\mathbf{F_{mag}} = V_f(\mathbf{M}\cdot\boldsymbol{\nabla})\mathbf{B} \quad 4\text{-}1$$

where $\mathbf{F_{mag}}$ is the magnetic force (N), **M** is the magnetization of the material (A/m), V_f is the volume of the magnetic entity (m^3) and **∇B** is the spatial variation of the magnetic field (T/m).

The laminar flow in a pipe is characterized by the Reynolds number that can be computed as

$$R_e = \frac{U_{flow}D}{\nu} \quad 4\text{-}2$$

where U_{flow} (m/s) is the fluid flow velocity in the main direction, D is the diameter of the pipe (m) and ν (m^2/s) is the kinematic viscosity of the fluid. In the case of a rectangular pipe, the equivalent diameter is the hydraulic diameter defined by

$$D_h = \frac{4A}{P} \quad 4\text{-}3$$

where A (m^2) represents the cross sectional area and P (m) the wetted perimeter. If R_e < 2,100 the flow in the pipe is considered laminar [80].

In addition, the viscous drag force that acts on a spherical particle is governed by Stokes' law when the spherical object is moving in a fluid and it is characterized by a low Reynolds number (< 1)

$$R_{e\text{-}p} = UD_p\nu^{-1} = 2Ur\nu^{-1} \quad 4\text{-}4$$

where $D_p = 2r$ is the diameter of the particle (m) and U is its velocity. Then the Stokes drag force is

$$\mathbf{F_d} = 6\pi\mu r\mathbf{U} \quad 4\text{-}5$$

where μ is the dynamic viscosity of the fluid.

In the case of a particle moving in a liquid, the magnetic force balances with the drag force [81] leading to the magnetically induced velocity

$$\mathbf{U_{mag}} = \mathbf{F_{mag}}\,(6\pi\mu r)^{-1} \qquad 4\text{-}6$$

Replacing Eq. 4-1 in Eq. 4-6 leads to:

$$\mathbf{U_{mag}} = V_f\,(\mathbf{M}\cdot\nabla)\mathbf{B}\,(6\pi\mu r)^{-1} \qquad 4\text{-}7$$

if all parameters are left constant with the exception of the size of the particle, the velocity acquired by the particle from the magnetic force in function of its radius is

$$U_{mag} = K r^2 \qquad 4\text{-}8$$

with

$$K = 2M\nabla B(9\mu)^{-1} \qquad 4\text{-}9$$

which clearly shows that increasing the size of the magnetic entity leads to an increase in the magnetic induced velocity proportional to the square of the radius of the particle [23].

On the other hand, we can state that the velocity of a particle in a flow and under the effect of a magnetic gradient is given by

$$\mathbf{U_{defl}} = \mathbf{U_{mag}} + \mathbf{U_{flow}} \qquad 4\text{-}10$$

where U_{mag} is given by Eq. 4-1 and U_{flow} is the velocity acquired by the particle due to the fact that is moving with the flow [39]. From Eq. 4-10 is clear that, if all other parameters are constant, the deflection pattern is governed by the fluid flow velocity.

Then, if Eq. 4-8 is re-arranged

$$U_{mag}\,\mu = \frac{2r^2M\nabla B}{9} \qquad 4\text{-}11$$

the product of the magnetophoretic velocity by the viscosity of the fluid is constant for a given particle in a given gradient. With which, by knowing the magnetophoretic velocity of the microparticle in water, there is a way to roughly estimate the magnetophoretic velocity of the particle in other non-aqueous media (e.g. blood) if the viscosity of the new fluid media is known

$$U_{new_media} = U_{mag_water}\,\mu_{water}/\mu_{new_media} \qquad 4\text{-}12$$

4.4.2 Particle tracking algorithm

Tracking is a non-trivial task, even in controlled environments. In order to evaluate the automatic detection and tracking of magnetic microcarrier aggregations, the OpenCV [82] library is used. The OpenCV library comes with a sample application called blobtrack [71] designed to track objects moving with respect to a static background. The general algorithm is described in [83], basically it performs a video frame segmentation, motion detection and trajectory update.

The input video frame is used to estimate the background. The background is then subtracted from the video frame. The resulting foreground frame is divided into regions that are grouped into connected components. By analyzing the connected components, it can be determined if each the region is: an existing object, a new object, there is a merge detected between objects, or there is a split detected for an object [84].

4.5 Experiments

4.5.1 Microparticles for magnetophoresis measurements

To characterize and validate the method and the proposed system, PS-MAG-S1986 microparticles from Microparticles GmbH (Berlin, Germany) were used in this study. These microparticles have a mean diameter of 41.13 μm, are monodisperse, and have a magnetization of 36 kA/m in a field of 1.5 T as typical found in clinical MRI scanners. Although not quite at saturation, the microparticles are considered at saturation magnetization for the purposes of this report.

These microparticles were also selected because they exhibit a diameter almost equivalent to the TMMC that have been successfully navigated in the hepatic artery of rabbit models with controlled release of the therapeutic agent in specific locations in the liver [4].

4.5.2 Microfluidic design and fabrication

The microfluidic chamber as depicted in Figure 4-1 is designed to be 6 mm wide by 7 mm long with a depth of 200 μm. It has two inlet channels and one outlet channel. One of the inlet channels is used to inject microparticles and has a width of 500 μm; the other inlet is used to

provide the main flow, and it has a width of 1 mm. The main flow channel is bifurcated into two branches of 500 μm in order to allow injection of microparticles in the middle of the main flow. Then two main flow branches of 500 μm are combined with the microparticles inlet channel to produce an input channel of 2 mm. The output channel width is 2 mm. The entrance and exit to the magnetophoretic chamber are done by widening and narrowing the channel width. All the system has rectangular cross section with a depth of 200 μm.

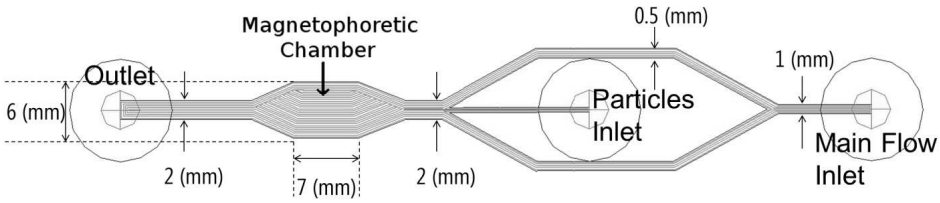

Figure 4-1 Schematic of the microfluidic device design. The complete device is 200 μm deep. Magnetophoretic chamber is 7 mm × 6 mm. Main flow and microparticles flow meet in the 2 mm entrance channel.

The microfluidic device was fabricated by milling the channels in a 1.5 mm thick poly(methyl methacrylate) (PMMA) sheet; the cover plate is another 1.5 mm thick PMMA sheet with access holes drilled on it. Both sheets are thermally bonded to form the microfluidic device.

The dimensions of the microfluidic chamber were selected such that a low Reynolds number is obtained for the fluid flow velocities used in the experiences. The hydraulic diameter Dh for the chamber is 387.1 μm, the maximum fluid speed used to perform the experiments is 20.8 mm/s, and the kinematic viscosity of water is 10-6(m2/s). By putting these values in Eq. 4-2, the maximum Reynolds number for the chamber is Re = 8.05 ≪2,100, which ensures laminar flow inside the microfluidic chamber for all the fluid speeds considered. The laminar characteristic of the flow was anyway investigated by injecting ink in the microparticles inlet as explained in [70]. The Reynolds number for a microparticle moving in the flow is Re_p = 0.05, which means that the Stokes law can be safely used for the case of individual particles.

4.5.3 Experimental setup

The magnetic suspension of microparticles has a concentration of 0.83 mg/ml and the suspending fluid is deionized (DI) water. The microfluidic device is placed in the center of the bore of a 1.5 T Siemens Avanto MRI scanner (Siemens, Erlangen, Germany) (Figure 4-2). A custom built Maxwell pair gradient coil is used to generate magnetic gradients. In this work, the gradient amplitude is always 400 mT/m. An MRI-compatible camera (MRC Systems GmbH, Heidelberg, Germany) is used to record the movement of the microparticles. The camera is located above the magnetophoretic chamber to allow monitoring the entrance of microparticles in the magnetophoretic chamber and records video at 15 frames/s.

Two syringe pumps are used to control the microparticles flows. The experiment is done by observing the deflection patterns at flow velocities of 2.6, 5.2, 10.4, and 20.8 mm/s. The microparticles are carried by the flow; therefore, if no magnetic gradient is applied, they travel in a straight line to the outlet. The microfluidic device is oriented such that the flow is perpendicular to the main static field B0 of the MRI scanner. The magnetic gradient is oriented parallel to the main static field.

The experimental protocol is as follows: start video recording, apply flow with the syringe pumps, as the microparticles are detected arriving to the magnetophoretic chamber turns on the magnetic gradient and when the microparticles finish its traveling through the magnetophoretic chamber, it turns off the gradient. The gradient is applied each time new microparticles arrive to the chamber.

4.6 Results

4.6.1 Experiments results

As mentioned above, the microfluidic chamber was tested in order to verify that at the fluid flow speeds considered, steady flow is expected. Figure 4-3 shows typical deflection patterns observed in each one of the flow velocities investigated. Each one of the inserted figures shown is formed by superposition of frames taken from the videos. For trajectories shown in Figure 4-3 the estimated magnetophoretic velocities are: for Figure 4-3a: 0.92 mm/s, for Figure 4-3b: 0.90 mm/s, for Figure 4-3c: 0.78 mm/s, and for Figure 4-3d: 0.95 mm/s. For more details refer to [70].

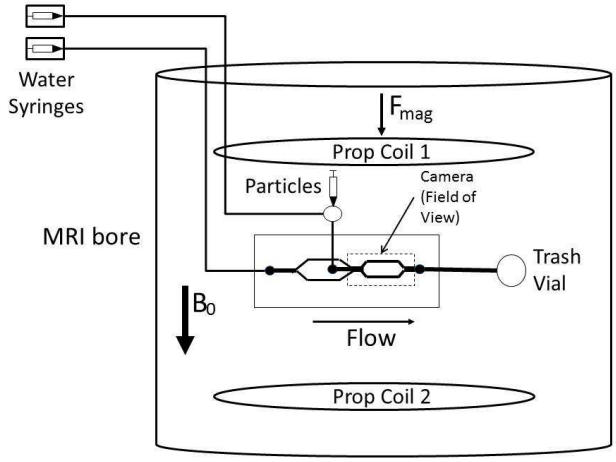

Figure 4-2 Schematic of the experimental setup. Prop Coil 1 and Prop Coil 2 refer to the custom Maxwell pair coils. It is seen that the fluid flow and magnetic gradient are intended to be orthogonal. Then all movement perpendicular to the flow is solely produced by the magnetic gradient from the propulsion coils.

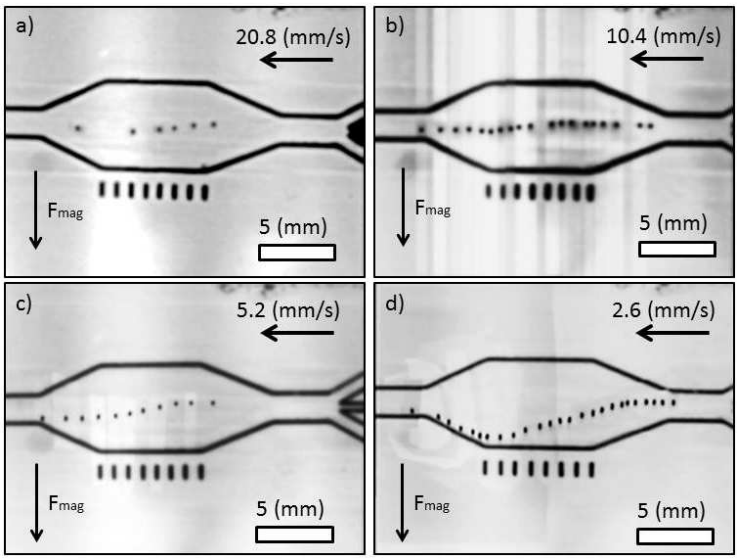

Figure 4-3 Effect of the fluid flow velocity on the deflection pattern of magnetic microparticles aggregations moving along the magnetophoretic chamber, in (a) the fluid velocity is 20.8 mm/s and it is difficult to notice the deflection of microparticles; in (b) the fluid velocity is 10.4 mm/s; in (c) fluid velocity is 5.2 mm/s, and in (d) it is set to 2.6 mm/s

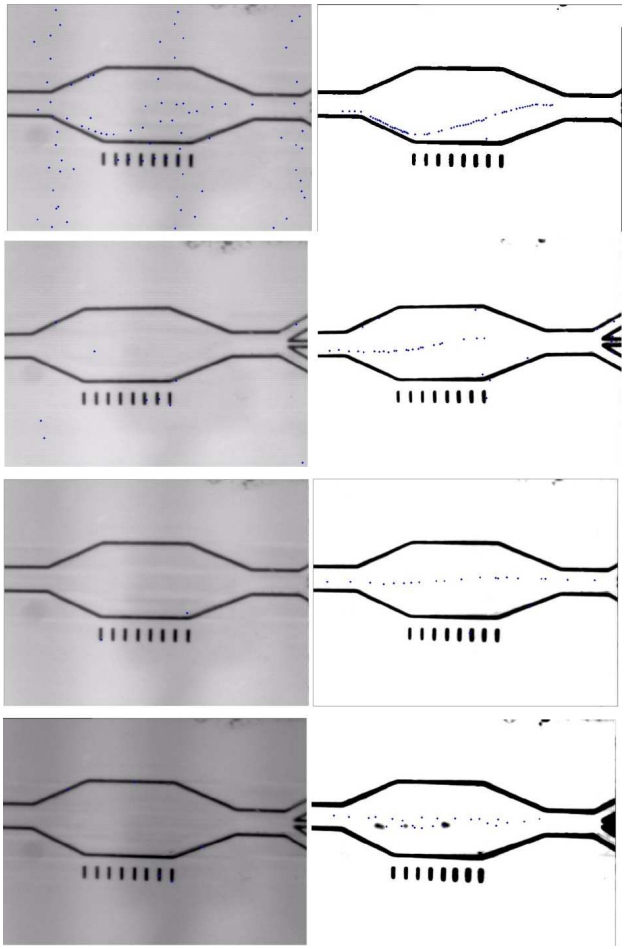

Figure 4-4 Comparison between the tracking software applied to raw video (left side) and to filtered frames video (right side). Only for the slower fluid velocity is possible to extract directly from raw video the trajectory of magnetic microparticle aggregations

4.6.2 Tracking experiments

The movies obtained in [70], used to initially estimate the magnetophoretic velocities of the magnetic aggregations, are used as a starting point to evaluate the option of using the OpenCV library to track and to compute automatically the magnetophoretic velocities of the microcarrier aggregations. Figure 4-4 shows the initial attempts with the raw videos obtained in the experiments, compared with the tracking done to the same videos but filtered before being treated for tracking and detection.

4.7 Discussion

As shown, the microfluidic device accomplished the task of allowing the observation of the magnetophoretic mobility for magnetic microparticles aggregations. However some limitations have emerged from the experiences. For instance, the magnetic gradient needs to be applied at the entrance of the magnetophoretic chamber otherwise the magnetic aggregations tend to follow the direction of the main flow. This means that if more than one aggregation reaches the microparticles inlet channel, those aggregations that have not reached the magnetophoretic chamber show a pronounced deflection pattern, but this behavior is due to the fact that microparticles aggregations get to the vicinity of the walls of the inlet channel and therefore follow the lines of flow from the main stream.

Another limitation of this setup is the fact that gravity is being neglected. The effect of gravity is not taken into account because the magnetophoretic chamber is studied from the top and vertical movements are not recorded. This limitation affects measurements especially at low flow speeds, because the more time the aggregations are in the magnetophoretic chamber, the more likely is that they are going to settle.

The mentioned limitations have not prevented us to get data on the way in which aggregations behave under different flow speeds. As mentioned above, we assume that aggregations are around the same size in each of the measurements done. The optical equipment used allows us to estimate aggregation sizes above 100 μm, but on the other hand, the size of aggregations seems to be limited by the size of the inlet used to inject them.

The initial results with the OpenCV library establish clearly the need of a calibration protocol before each one of the experiences in which characterization data is going to be gathered. The adjustment of contrast and brightness must be performed initially, followed by a step to learn the background such that the recognition of the moving objects that are going to be tracked and that belong to the foreground becomes more easy and accurate. This background learning process seems clear from the first couple of images in Figure 4-4 in which becomes apparent a spatial regular noise that the software recognizes as particles someway appearing in vertical positions, which could be attenuated with an appropriated spatial low pass filter. It seems clear also that a higher speed video camera would produce much better results, even though it could mean process the video data sometime after instead of in an immediately manner. As the

testbench is intended to evaluate the magnetic characteristics of the micro-entities before they are to be used as treatment and/or diagnostic vectors, this last limitation appears to be minor. It is more important to get the right data than to get it earlier.

Another way to cope with the problems of the video quality could be to use lower fluid flow velocities in order to detect and track the aggregations safely. Considering that fluid flow velocities less than 2.6 mm/s are far from blood flow velocities in some of the more important arteries [73], this last option needs to be evaluated carefully. The importance of the testbench protocol design is to reflect as closer as possible the deflection patterns that the magnetic microcarriers are going to show inside real vascular environments in patients.

4.8 Conclusions and future work

In this study, a microfluidic device has been designed to evaluate the effect of the fluid flow velocity on the deflection pattern of magnetic aggregations. Preliminary results show that this device allows magnetophoretic velocity estimations at different fluid flows, and thus, allows characterizing drug or diagnosis magnetic microcarriers containing different magnetic nanoparticle content. Even though the detection and tracking of the microparticle aggregations in situ is still challenging, post processing of the data could cope with this limitation. Fundamental investigations on this specific subject are usually theoretical and experimental data could lead to new applications of microcarriers. This is the first step in the direction to produce a testbench for micro-entities to be used in MRN. The knowledge about microcarriers' deflection patterns should allow better predictions of targeting efficacy.

Future work includes other magnetophoretic chamber designs with the microparticles' inlet being positioned such the magnetic gradient does not need to be synchronized with the entrance of particles or aggregations to the magnetic chamber, a design inspired from the work done in [39]. Another interesting chamber design to try is one based on the work from Carr *et al*. [85], in which the microfluidic chamber is positioned vertically instead of horizontally, a way in which friction forces with the walls of the microfluidics related to settling of particles is avoided.

It is necessary also to verify the behavior of magnetic aggregations when the gradient force is applied perpendicular to the main field. Some simulation studies suggest that the angle of the chain like aggregation with respect to the gradient could play an important role in targeting

efficiency [76]. As microfluidic magnetophoretic chambers are used for separation and sorting purposes, the next generation of devices will include several outlets to estimate the fraction of aggregated versus non aggregated microparticles.

In parallel the detection and tracking system, including the software tools and experiences protocol, must be refined to allow improved data gathering on the deflection trajectories. Finally for the tool to fully accomplish its use, a magnetic microcarriers' database must be designed to collect the data obtained. In this respect a relational database design (SQLite [http://www.sqlite.org/]) and object-oriented approach (db4o [http://www.db4o.com]) are under consideration due to the requirements of the system.

4.9 Acknowledgments

The authors would like to thank particularly Charles Tremblay, Ke Peng, Alexandre Bigot, Nina Olaemei, Viviane Lalande, and Manuel Vonthron from NanoRobotics Laboratory, for their suggestions and their support to this project. The blobtrack sample code used in this work was initially modified and tested by Behnam Izadi.

CHAPTER 5 PROPOSED TRACKING METHOD

As the OpenCV blobtrack application was already used in other project in the laboratory, initially it was reused as the data gathering tool when tracking microparticle aggregation movements in the magnetophoretic chamber. In this chapter the blobtrack application initial trial usage is described. Then, taking into account the lessons learned, a new tailored tracking tool based in a translational model is proposed and initial results of its use are presented.

5.1 Tracking using OpenCV blobtrack

As mentioned in Chapter 3, the blobtrack application from OpenCV was used to evaluate the automatic detection and tracking of magnetic microcarrier aggregations. The general algorithm is described in [83], basically it performs a video frame segmentation, motion detection and trajectory update. The input video frame is used to estimate the background. The foreground/background differentiation algorithm used in the blobtrack application is the one presented in [86]. This method is based on a Bayes decision rule applied to probability density functions assigned to the pixel values. The background image is updated gradually from the input image sequence by assuming that pixel values have relatively few changes for stationary backgrounds and that pixel value changes for moving background are similar and happen in the same place of the image [86]. The background is then subtracted from the video frame. The resulting foreground frame is divided into regions that are grouped into connected components. By analyzing the connected components, it can be determined if each the region is: an existing object, a new object, there is a merge detected between objects, or there is a split detected for an object [84]. The algorithm used for foreground segmentation is described in [84] and is implemented using the OpenCV contour finding function based on [87]. A contours list is generated, according to size too small blobs are removed, others are removed if there is intersection between them (the track is done to just one of them until they separate enough) and the same distance measure is used to detect new objects [84]. The distance measurements used to detect intersection between blobs are represented in Figure 5-1. If the distance between the centroids of the blobs is less than the sum of the halves of their widths and heights, then they intersect. Finally the list of blobs is bubble sorted and only the first 10 biggest blobs are kept.

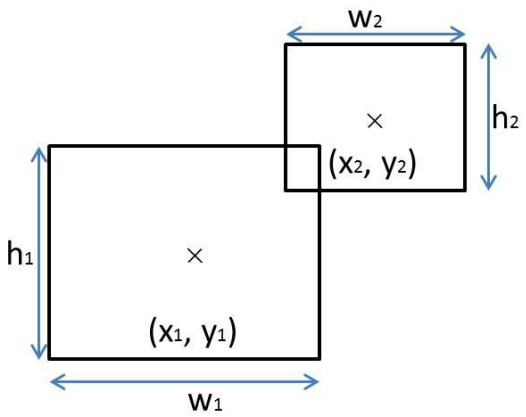

Figure 5-1 Distance measurement to detect blob intersection. The quantities $d_1 = x_2 - x_1$ and $d_2 = y_2 - y_1$ are horizontal and vertical distances between centroids of the blobs, w_1, w_2 are the widths and h_1, h_2 are the heights of the blobs respectively. If $d_1 < (w_1/2 + w_2/2) \wedge d_2 < (h_1/2 + h_2/2)$ the blobs are considered merged.

By default, the blobtrack application uses two methods to track object position and size: a simple connected-component tracker and a more complex tracker based on a hybrid implementation of a particle filter weighted by mean-shift measurements. Mean Shift algorithm is an iterative procedure that looks for maximize a similarity metric, which usually is the Bhattacharryya coefficient [88]. In particle filtering the objects are represented as state variables, the aim of the algorithm is to estimate the state of the object given previous state measurements, a weighted sample set is used to represent conjectured object states [89].

In Figure 5-2, the detected aggregations in different frames alongside with the calculated foreground (resulted from subtracting the background to the current frame) are shown for the fluid velocity. In this figure it can be noticed that some illumination problems caused noise that could result in spurious detected particles. The source for the illumination problem can be attributed to the fact that inside the bore of the MRI scanner some vibration is induced by the cooling system of it. This vibration caused the illumination slightly and periodically change, and these changes were interpreted by the tracking software as new objects. In Figure 5-2 there was two chain like aggregations, one moving from left to right (the highlighted one) and another one at a standstill positioned left from the first one. The tracking software is expected to detect only

the moving chain like aggregation, and maybe, the stand still one. All other detected objects are due to noise.

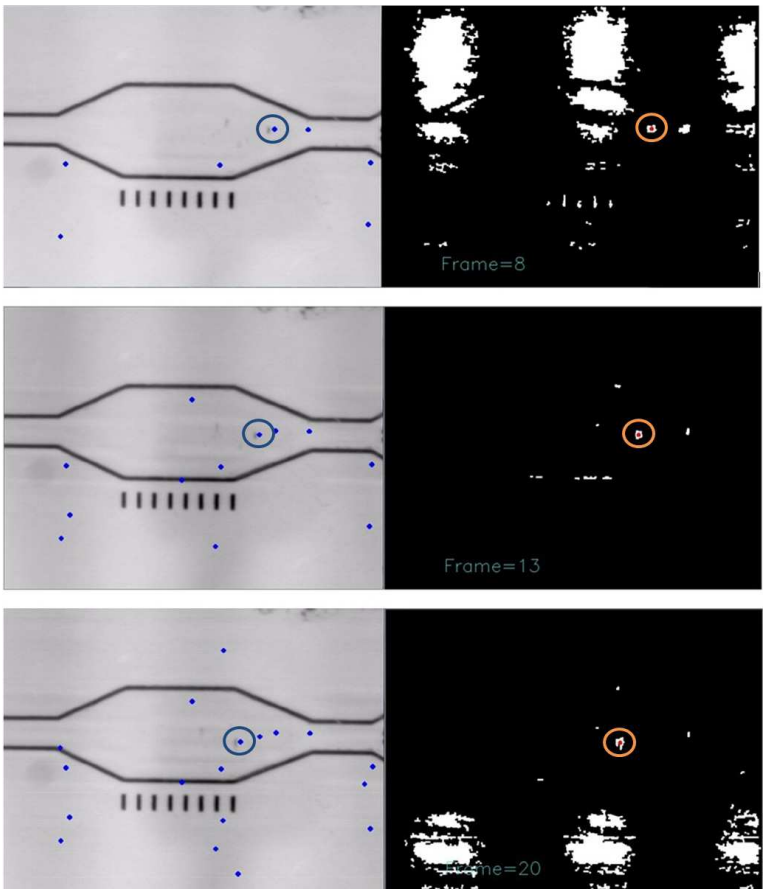

Figure 5-2 Detected aggregations in different frames. Accumulated detected particles at different points in time are shown at left. Foreground resulted by background subtraction from current frame is shown at the right. The video used is the one at which the fluid velocity is 2.6 mm/s. Particles detected are highlighted with a circle surrounding them.

The blobtrack application is primarily intended for general surveillance applications. Then it contains several modules with algorithms that were not used for this project. In order to get better results in identifying chain like microparticle aggregations a prefiltering process was designed. The process followed in a frame basis is: decrease brightness (by using cvAddS function), increase contrast (by using cvScale function), simple mean filter smoothing (cvSmooth with CV_BLUR option) and binary thresholding (cvThreshold with CV_THRESH_BINARY).

Blur smoothing is used to reduce the effect of noise in images, and thresholding is used in order to eliminate, as much as possible, image artifacts that could be interpreted as particles. In the case of higher fluid flow speeds, the software is not able to track the magnetic microparticles aggregations, even when the human eye is capable to distinguish their movement. In this case the microparticles were marked by hand. The results are shown in Figure 5-3 for the same frames as in Figure 5-2. The first column shows the result of reducing brightness in frames 7, 13 and 20. The second column shows the result of increasing the contrast in frames 7, 13 and 20; it is interesting to note that chain like aggregations seem less visible in this step. The next step applied to mentioned frames is shown in Blur column with the smoothing process intended to enhance chain like aggregation appearance by making more uniform the regions of relative similar color. The final column shows the thresholding process by which chain like aggregations are more easily highlighted.

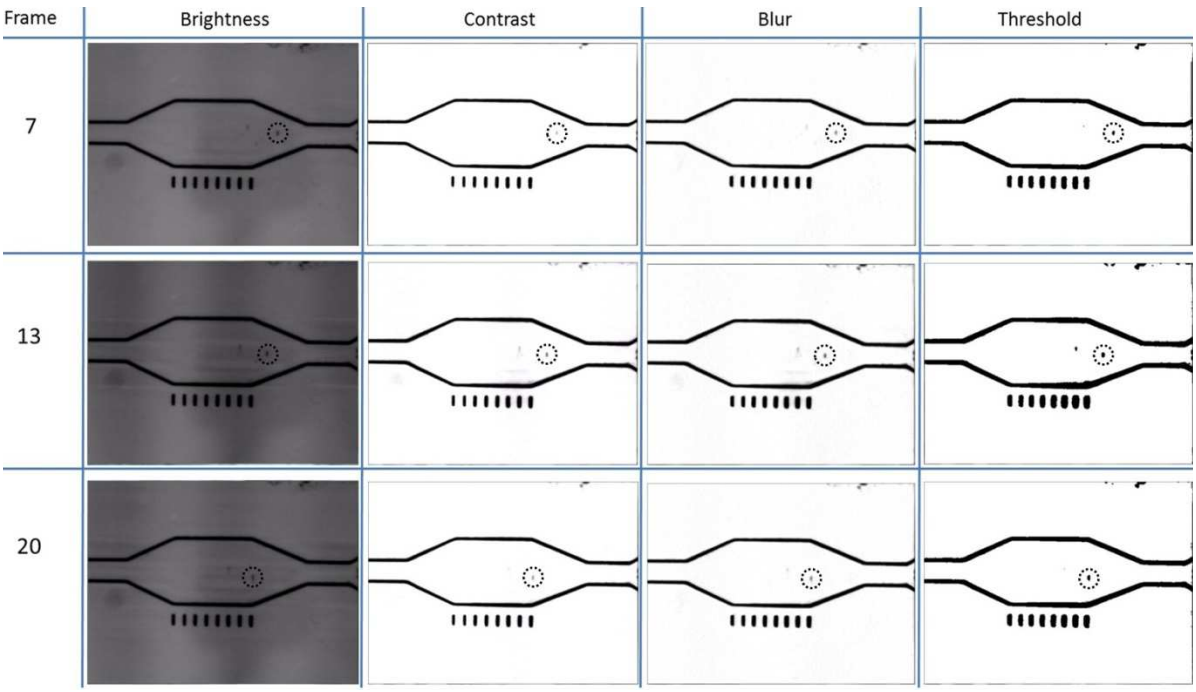

Figure 5-3 Filtering process example applied on the same frames as in Figure 5-2. The tracked aggregation is highlighted by encircling it to show the effect of each filter step.

Based on the results obtained and the knowledge acquired, a new graphics interface for data acquisition was designed. This tracking application is developed using Qt [90] for user interface design and OpenCV [82] for image processing. As large quantities of data are expected to be collected from each of the magnetophoretic characterization experiences, more tailoring is added to the tracking process.

5.2 Tracking tool description

The new object detection and tracking software implementation is designed to be simple, and then some assumptions are made. The first assumption is that the user of the tracking software knows a priori the fluid flow speed at which the magnetophoretic experience has been made. This information is key for the well-functioning of it, because it is used to estimate the motion of magnetic aggregates. The second assumption is that the user knows or is able to indicate to the software a region of known physical size. This information is used to estimate the magnetophoretic velocity in terms of real physical quantities.

In the new software implementation, in the first step the user can select and open the file containing the video with the recorded experience. In the next step the user must enter the fluid flow speed used to perform the experiment as shown in Figure 5-4. During the opening of the video file, the frame rate is automatically saved by OpenCV opening video function.

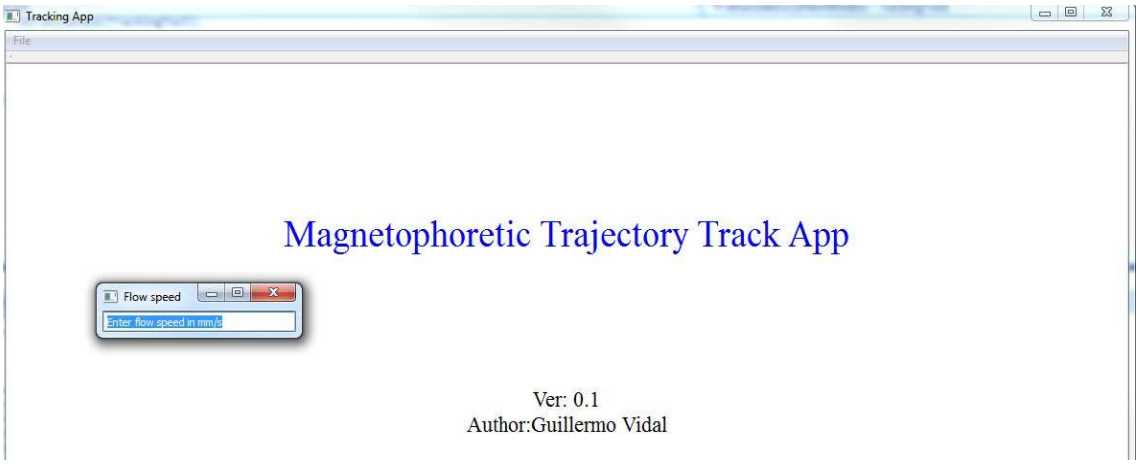

Figure 5-4 Window to enter fluid flow speed used in the opened video.

The following step allows the spatial scaling of images. In the current software version it is assumed that pixels have a square shape, and then horizontal and vertical sizes are the same. Spatial calibration is used to calculate the conversion factor between pixel dimensions and physical real-world ones. In order to do so, the user has to define an area of known horizontal size; as shown in Figure 5-5. The vertical black lines shown in Figure 5-5 were designed with spatial calibration in mind; these lines are evenly spaced, separated by 1 mm between each other. Therefore they represent the length of the magnetophoretic chamber, i.e., 7 mm. These lines belong to a paper sheet that is placed below the microfluidic device. In Figure 5-5 a) is shown the message presented to the user to ask for draw a rectangle with known horizontal size. In Figure 5-5 b) the rectangle has been drawn over the spatial calibration black vertical lines and the user is asked to enter the horizontal size of it (in mm); in this case 7 mm. In Figure 5-5 c), the user is shown with the resulting conversion factor, which in this case is 27 pixels/mm (or equivalently 37 μm/pixel).By having this conversion factor is possible to calculate velocities and other quantities in physical units in the next steps.

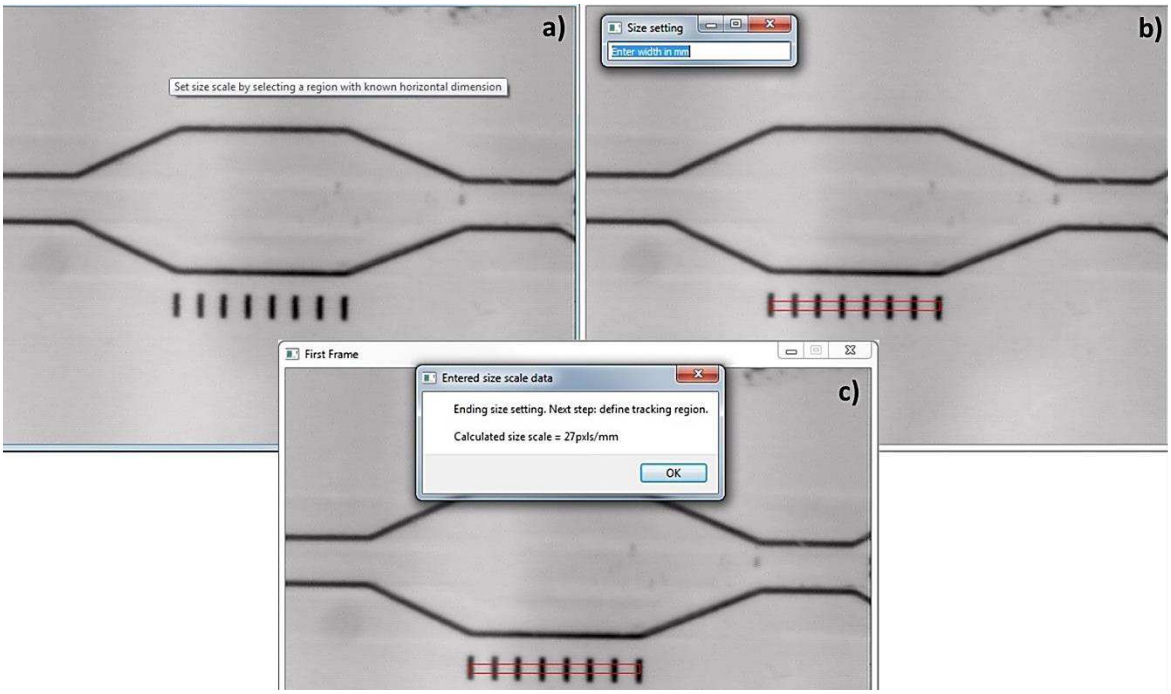

Figure 5-5 Spatial calibration. Selection of a region of known horizontal size that is used to calculate the equivalent size in pixels, in this case the result is 27 pixels/mm.

The user is then prompted to select the tracking region, in this way it is possible to save computing resources; this step is shown in Figure 5-6. In Figure 5-6 a) the user is shown a message indicating that he has to select the tracking region. In Figure 5-6 b) the user is asked to confirm that the tracking region is correct. This step allows the user to change the tracking region if it has not been selected properly. Once the tracking region is selected, the video is loaded and the tracking process starts.

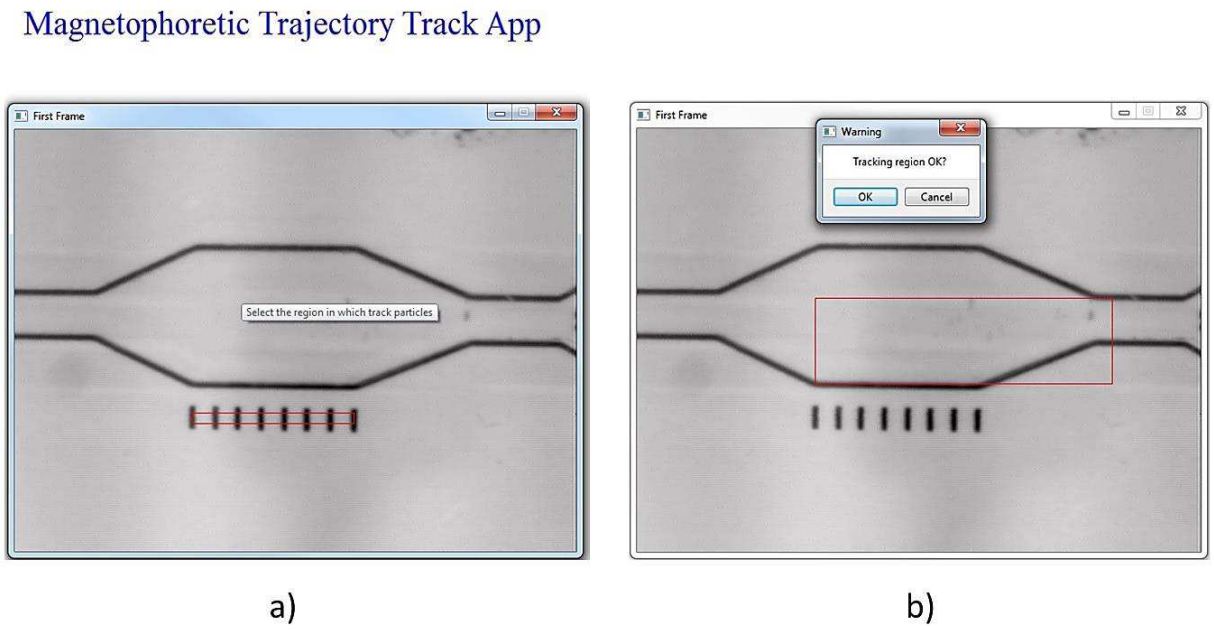

Figure 5-6 Tracking region selection. The user can define the region in which the tracking is to be performed.

5.2.1 Frame processing

The flowchart of the preliminary tracking process is summarized in Figure 5-7. As indicated in Chapter 2, the first step is to detect objects in each frame. As mentioned in Chapter 3, the recorded videos have illumination problems.

The video is accessed frame by frame in a loop that ends when no more frames are available. Frames are imported using the OpenCV query frame functionality. The frames are stored as an IplImage structure. It is possible to use a camera to feed a videostream instead of just opening a saved video file.

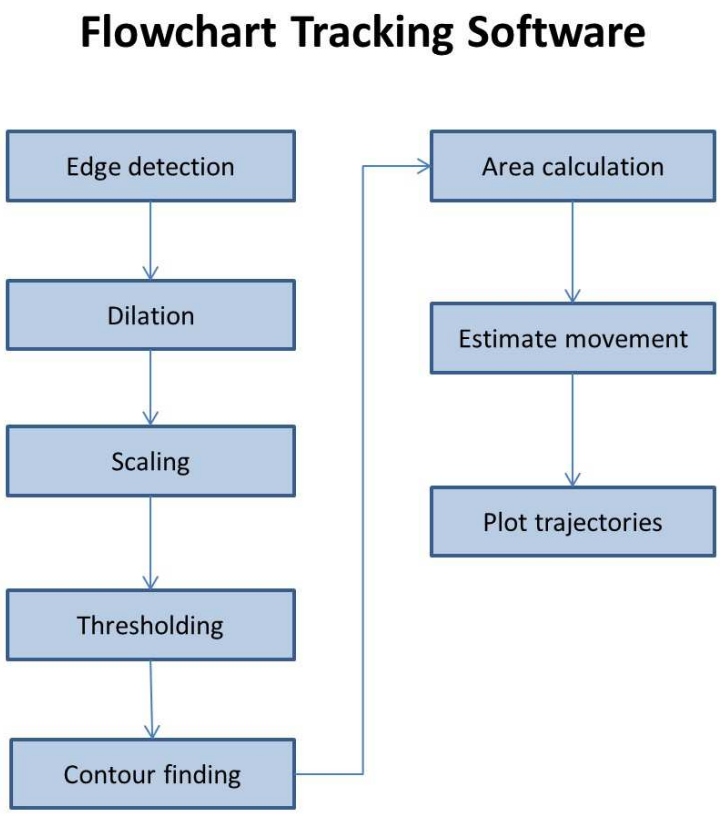

Figure 5-7 Simple flowchart of the preliminary tracking software.

Due to the fact that magnetic microparticle aggregations have chain-like shapes, a Sobel filter is applied to detect vertical edges in the selected tracking region (Figure 5-8a)). One the effects of using this filter is that horizontal lines are eliminated. In Figure 5-8a) is shown the result of using this filtering step on a region defined in the previous step that included the black horizontal drawn line used to better visualize the edges of the magnetophoretic chamber. This horizontal line is not present in Figure 5-8a), because the filtering process has eliminated it. In this way fewer false positive objects are detected. The resulting image includes a long diagonal line in the right-bottom corner, which corresponds to a black drawn line used to delimit the edges of the microfluidic chamber. It also includes a portion of the corresponding diagonal line delimiting the other part of the magnetophoretic chamber, which is seen in the left bottom corner. The chain like microparticle aggregation is the vertical line in the right-top corner in Figure 5-8a).

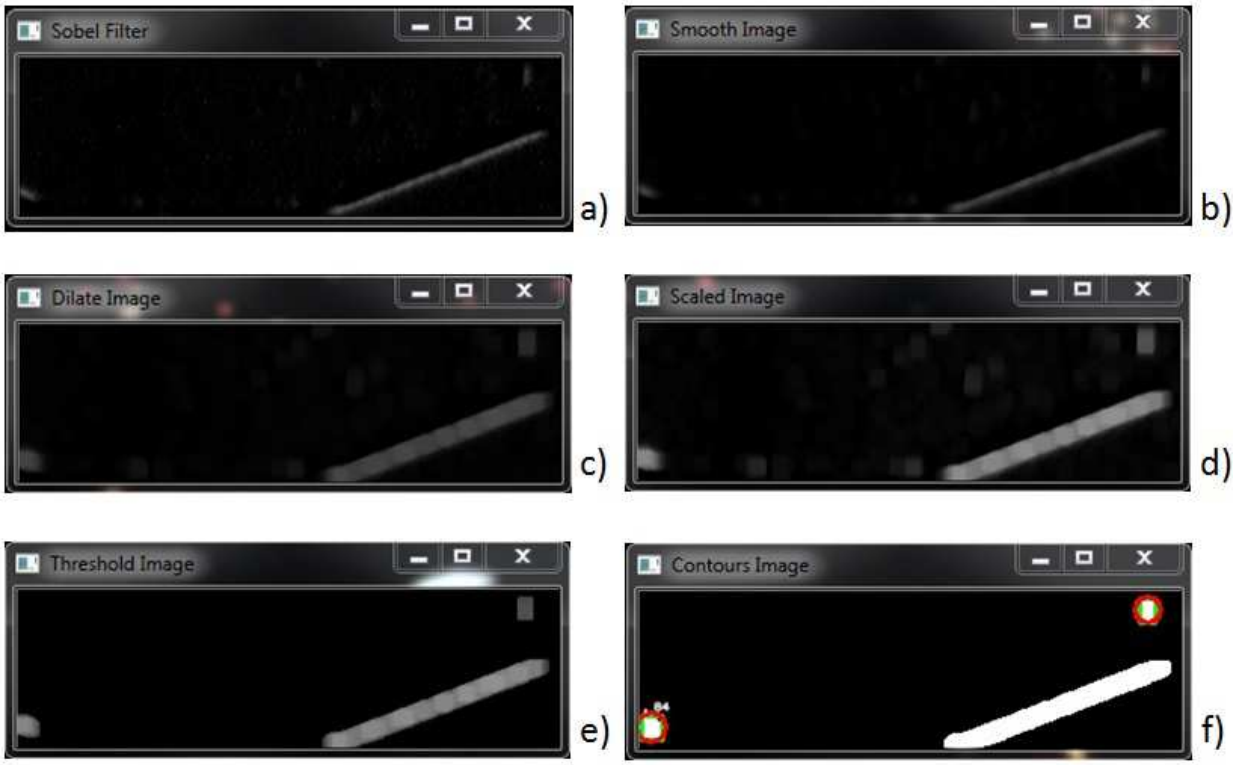

Figure 5-8 Image processing prior to tracking.

In order to remove noise, the function cvSmooth is used to perform a median filter (Figure 5-8b)). The smooth process using the median filter depends on the selection of the appropriate filter window size. For the frames shown here the median filter window size selected is 3×3. In future evolutions of the tracking tool, the size of the window used for the median filter is to be adjustable. The window size affects the quality of the smoothing process. The use of the median filter for the smoothing process was due to the fact that has the ability to usually preserve edges better than other smoothing techniques.

The resulting image is dilated in order to increase the size of the zone where aggregations are (Figure 5-8c)). As at this time the actual size of aggregations is not being determined, dilation can be safely used because the centroid of the dilated magnetic microparticle aggregations is conserved. As we are interested in calculating the magnetophoretic velocity, the centroid of the aggregation is used to estimate the magnetophoretic speed. The dilation process is done 3 times with a 3×3 structure element.

In the next step the resulting image is re-scaled to make the aggregations easier to identify (Figure 5-8d)). The re-scale process is simply the multiplication of each pixel in the image by 2 (in our case). In this way, the contrast in the image is incremented by making the aggregations and other elements in the frame brighter than the background. One problem generated in this step is that the noise also gets and increased contrast.

In order to eliminate noise generated in the precedent step, thresholding is applied. After some tests it was found that making 0 to every pixel value less than 50 produced the best result for the video sequences discussed here (Figure 5-8e)), in the sense of preserving microparticle aggregations while making other artifacts be part of the background.

The process described here is repeated with each frame in the video to be processed. The final result includes the drawn diagonal lines used to mark the edges of the microfluidic chamber (bottom portion in Figure 5-8e)) and the microparticle aggregation (top portion in Figure 5-8e)).

In the next step the object detection is performed by using the function cvFindContours that returns the number of retrieved contours and a pointer to the first one. The retrieved contours are processed by calculating their area; each contour that belongs to a window of permitted area values is saved in an array. This array contains the contours that are the moving object candidates for tracking. The Figure 5-8f) shows the possible moving objects detected in the first frame for the 2.6 mm/s movie used in Chapter 3.

5.2.2 Motion estimation

In the final step the movement of the magnetic microparticle aggregations is estimated by using the flow speed that the user has entered to define a search window in the sense of the flow. To do so a simple deterministic translational model is used, in which if I_n and I_{n-1} are the horizontal positions of the object in the frames n and n - 1 respectively they are related by:

$$I_n = I_{n-1} + \delta \tag{5-1}$$

where δ is the displacement that defines the position around which the search area is set in the next frame, and can be computed as:

$$\delta = \frac{U_{flow}\, Scale}{FR} \tag{5-2}$$

where U_{flow} is the user-entered fluid flow speed, *Scale* is the calculated equivalence between distance and pixels, and FR is the automatically obtained frame rate of the video sequence.

Another common displacement model is given by the Kalman filter method that uses the state space approach; it is intended to deal with noise and random perturbations that usually occur in real video data. This method is more accurate and robust than the translational one, but uses more computational power. The goal of this project is not to provide a way to estimate all possible particle movements and a simple deterministic translational model can be safely used due to the fact that microparticle aggregations are expected to follow fluid flow lines in its horizontal displacement. It is also supposed that only one object is moving between frames. The control of bolus injection goes beyond the boundaries of this thesis.

If a particle is found inside the search window, the vertical position is verified to eliminate the possibility of noise being detected as a particle, or another particle being confused with the tracked one. The results obtained with this approach are shown in Figure 5-9 for the 2.6 mm/s video in which 2 particles are detected and the speeds are calculated. In this case the second particle is just noise, while the first particle is the main magnetic aggregation that is moving in this sequence. One thing to notice is the speed estimated by the software. The fluid flow is expected to be 2.6 mm/s, but the calculations based on tracking of the aggregations results in 3.3 mm/s. On the other hand, the magnetophoretic speed estimated in this case is 0.7 mm/s, which is much less than the initially estimated one. One of the reasons for this could be the fact that the speed is being estimated by calculating the total vertical distance traveled during the entire tracking time. In this specific case, the aggregations are moving in several frames only due to the fluid flow, then after some frames the magnetic gradient is applied. Then the magnetophoretic velocity could be under-estimated in this case. The result of applying the tracking software to the movie in which the fluid flow is 5.2 mm/s is shown in Figure 5-10.

Following up of the movement of magnetic aggregations by human eye was possible in the videos collected during experiences, but automatic tracking proven to be difficult as the aggregations were clear only at the lowest speeds. This preliminary tracking software development shows that the magnetophoretic chamber designed can be useful to characterize magnetic microentities intended for the use in MRN. Of course more work needs to be done in order to get a fully working testbench. One of the main limitations of the set-up is the low-speed

camera used (15 frames/s with a higher limit of 30 frames/s). A higher-speed higher-resolution camera should produce videos easier to track, implying that more data needs to be treated.

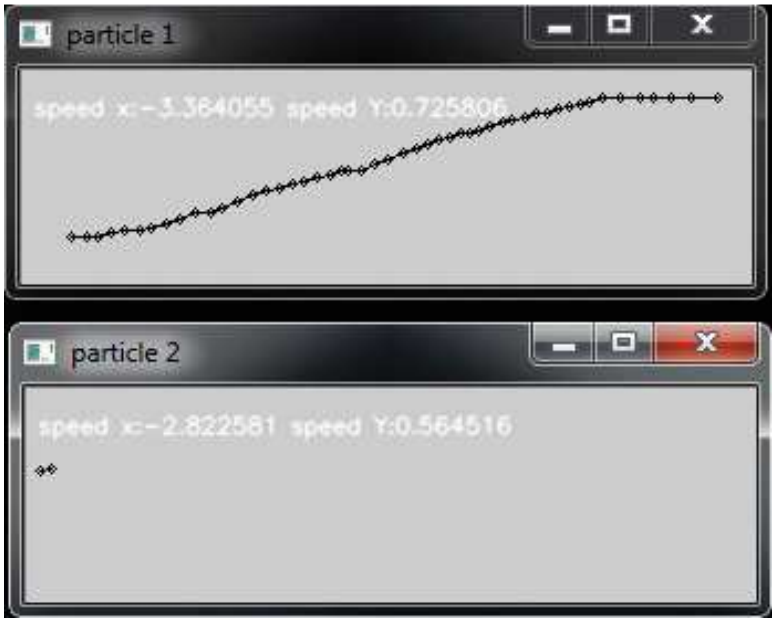

Figure 5-9 Deflection pattern of aggregations in 2.6 mm/s movie.

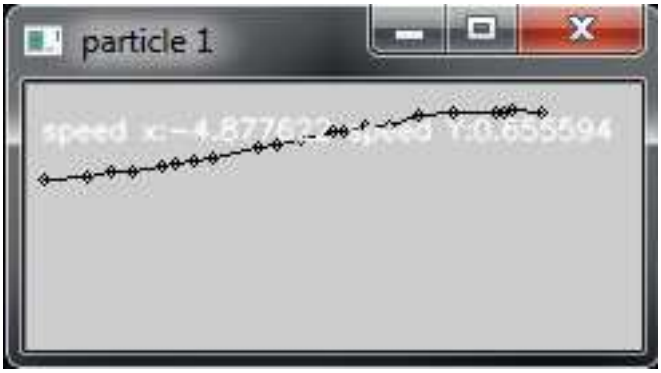

Figure 5-10 Deflection pattern of aggregations in 5.2 mm/s movie.

Finally, as mentioned in [59], there are a lot of tracking tools available commercially and freeware, but often image data must satisfy conditions that are usually violated in experimental environments, which in turn provoke the tracking to fail. Next generation of the tracking software for measuring magnetophoretic attributes must include tools to allow the modification of obtained images (image preprocessing could be interactive) and trajectories.

5.2.3 Location accuracy

In order to assess the accuracy of the tracking method proposed here for magnetophoretic experiences, simulated videos were generated in MATLAB with known trajectory data.

The videos were generated assuming that the magnetic aggregations have a spheroid shape. The speeds in X range from 1 to 20 pixels/frame, and in Y a constant velocity of 2 pixels/frame is used. In order to investigate the effects of noise on the performance of the tracking software, new videos were generated starting from the basic initial one. The first source of noise is a spatial illumination variation; this variation is, by now, only in terms of columns in the generated images. Starting from these 2 videos, Gaussian white noise with known σ is added in order to generate image sequences with predefined signal to noise ratio (SNR). The SNR used in this project is defined by

$$SNR = 10 \log_{10} \frac{\sigma_{gt}^2}{\sigma_n^2} \qquad 5\text{-}3$$

with σ_{gt}^2 and σ_n^2 the varianzas of the image without noise and of the noise itself. Eq. 5-11 is used to compute the varianza strating from a known SNR.

The SNR range was logarithmic with 10 steps starting with a value of 0.1 dB up to 39.8 dB. For the case of videos without spatial illumination noise, in all cases the maximum error in determining the centroid of the ellipsoid was 1 pixel in the *x* and *y* axis. However when the spatial illumination noise was added, only in the case of SNR bigger than 20 dB, the tracking software is capable of correctly determine the centroid of the simulated aggregation.

These experiences indicate that with good quality video sequences, it is possible to obtain accurate data on the movement of magnetic aggregations in the magnetophoretic chamber. The spatial illumination variation can be attenuated by using the appropriate filter prior to the tracking process.

The long term goal of these measurements it is to provide the data to populate a database containing main magnetic microcarrier characteristics. This database is expected to be accessed by the MRN core software to provide the medical team with suggestions about the better magnetic navigable entity to be used in a specific situation.

This data could also provide the means to estimate the outcome of the MRN treatment. For instance, in [91] a stochastic model is proposed to predict the behavior of a system of microrobots powered by bacteria. The stochastic model defines a series of macroscopic parameters that are determined by using movement experimental data. Then, if a similar model is defined for MRN treatments, the outcome of magnetocphoretic experiences could be used to estimate similar macroscopic parameters and then predict the targeting efficiency.

CHAPTER 6 GENERAL DISCUSSION

This chapter includes a discussion on the methodology used and possible improvements at experimental and software levels.

6.1 Experimental setup

As usual in microfluidics, in the project it was assumed the non-slip boundary condition, which states that a fluid in contact with a stationary boundary has zero velocity. This implies that when particles settle they should stop moving and then should not contribute to the calculation of the magnetophoretic velocity, then if microparticles aggregations are moving, we are assuming that they have not settled yet. However, it is more likely that settled microparticles will roll due to the force exerted by the fluid, and this effect is difficult to compute. In order to avoid this effect, some solutions exist. One way to avoid settling effects is by changing the viscosity of the fluid in order to increase the settling time. If this solution is used, it is necessary to study the validity of Eq. 4-12, but in the case of chain-like aggregations.

Usually the magnetic chain like aggregation shape is approximated by cylindrical or ellipsoid geometries [55, 76]. If the ellipsoid geometry and low particle Reynolds number for magnetic particle aggregation chain like are assumed, the drag force on it can be written in terms of a correction factor [92] for the drag force on an equivalent sphere

$$\mathbf{F_{d_agg}} = 6 f_E \pi \mu r_e \mathbf{U} \tag{6-1}$$

where f_E is the Stokes correction coefficient and r_e is the radius of the equivalent sphere with the same volume as the ellipsoid. The correction coefficient f_E depends on the aspect ratio E of a spheroid given by

$$E = \frac{d_{||}}{d_{\perp}} \tag{6-2}$$

with $d_{||}$ the length of the semi-axis parallel and $d_{\perp}$ the length of the semi-axis perpendicular to the symmetry axis of the spheroid, in Figure 6-1 the semi-axis are schematically represented for a prolate ellipsoid case. The values for the coefficient f_E in function of E can be found elsewhere [92].

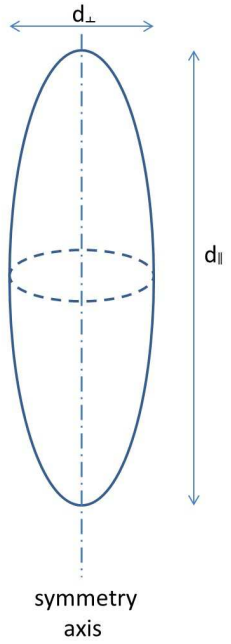

Figure 6-1 Prolate ellipsoid representing magnetic chain-like aggregation shape.

As mentioned before, the Reynolds number for a moving particle (or aggregation) in a fluid flow is given by:

$$R_{e\text{-}p} = UD_{ep}\nu^{-1} = 2Ur_{ep}\nu^{-1} \qquad 6\text{-}3$$

with $D_{ep} = 2r_{ep}$ the diameter of the equivalent sphere particle. Eq. 5-1 is only valid if $R_{e\text{-}p} \ll 1$, then if we suppose that D_{ep} is 300 µm and if the fluid has the kinematic viscosity of water (1×10^{-6} m^2/s), the translational speed of the aggregation due to the applied magnetic force must be much less than 3 mm/s (which is the case in our experiences). If the kinematic viscosity is augmented, the maximum deflection speed of magnetic particle aggregation also increases. For example, if the kinematic viscosity of the fluid is designed to be the one of blood: 3.3×10^{-6} m^2/s, the magnetic particle aggregation must reach a velocity much less than 11 mm/s, which is the case in our experiments.

Again magnetic and drag forces balance, so the magnetically induced velocity on the aggregation is:

$$\mathbf{U_{mag_agg}} = \frac{V_{f_agg}(\mathbf{M}\cdot\nabla)\mathbf{B}}{6f_E\pi\mu r_e} \qquad 6\text{-}4$$

where V_{f_agg} is the volume of the ellipsoid shaped aggregation. Rearranging Eq. 5-4 we could estimate that

$$U_{mag_agg}\mu = \frac{2r_e^2 M \nabla B}{9\ell_E} \qquad 6\text{-}5$$

is constant for a given aggregation in a given gradient, if the Reynolds number of the magnetic microparticle aggregation is low. Usually glycerol-water mixtures are used to get higher viscosities while keeping a density similar to water [93] (e.g., a mixture with 60% of pure water and 40% of glycerol is usually used to simulate blood viscosity).

Neutrally buoyant microparticles can be used to estimate the coefficient of friction experienced by magnetic particles by comparing the navigation of both specimens without the influence of the magnetic force. Neutrally buoyant microparticles are expected to not sediment and follow the streamlines of fluid flow. This also can be used to better calibrate the fluid flow speed and to investigate the laminarity of the fluid flow in the magnetophoretic chamber.

On the other hand, it is also possible to perform the experiences by placing the microfluidics device with fluid flow and gravity in parallel; in this case the effect of gravity must be included in the deflection equation. The aggregations and microparticles should never interact directly with the wall surfaces in this case. This solution is relatively simple but does not allow an easy study of the effect of the angle between chain like aggregations and magnetic field gradient in the magnetophoretic response.

As mentioned in [10, 70] the microfluidics design can be improved to facilitate the repeatability of experiences. In the current design, if the magnetic force is turned on before the magnetic aggregations have reached the magnetophoretic chamber, the trajectory followed by them is too pronounced; this situation is represented in Figure 6-2 in which green aggregations have been propelled too early.

It is also desirable that the new design has several outlets. The process of magnetic aggregation is complicated and depends on several factors as magnetic particle concentration, magnetic content in the microcarriers to mention some. It is expected that most of the magnetic microcarriers should aggregate, but some of them would remain unaggregated. The ratio of aggregated and unaggregated magnetic microcarriers directly influences the targeting effieciency. It is more likely that aggregated microparticles are going to respond as expected to the applied

magnetic gradient. With a multiple outlet magnetophoretic chamber it could be possible to estimate the fraction of aggregated magnetic particles for given experimental conditions. By knowing this ratio, it is possible to better estimate how much of the therapeutic agent could reach the tumor in similar conditions and the treatment planning could be done accordingly.

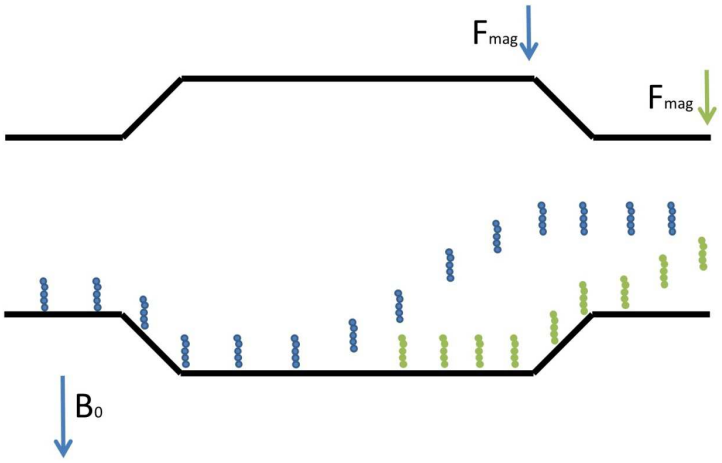

Figure 6-2 Current chamber design problem. Aggregations represented in blue are subjected to the magnetic gradient at the right time. In green is represented the situation when the magnetic gradient is turned on too early.

Due to the size of the magnetic microparticles used in this experience, Brownian motion induced by thermal energy can be safely ignored. In effect, the dimensionless Péclet number measures the relative importance of diffusive transport (due to Brownian motion) versus convective transport

$$P_e = \frac{U_{flow} D_h}{D} \qquad 6\text{-}6$$

with the diffusion coefficient D given by Stokes-Einstein's expression:

$$D = \frac{k_B T}{6\pi\mu r} \qquad 6\text{-}7$$

where k_B is the Boltzmann's constant and T is the absolute temperature. If Pe $\gg$ 1, diffusion is considered absent and microparticles follow flow lines [94]. In our case supposing a temperature of 20 °C, and using the particles radius of 40 µm and the minimum flow speed of 2.6 mm/s, the

Péclet number results in 9.8×10^7 as worst case, which indicates that Brownian motion is negligible compared with convective transport and magnetic microparticles can be considered following fluid flow streamlines.

In [95] it is mentioned that the distortion in fluid flow caused by the movement of a microparticle can induce a drag force into other ones, and so affecting their trajectories. This effect has been neglected but maybe it could be important to asses it in future developments.

As it has been mentioned before, one of the main problems of the current setup is the fact that the effect of gravity is being neglected. The use of higher viscosity fluids is discussed as a possible solution. A different disposition of the setup such the movement of the magnetic aggregations could be parallel to the gravity is also discussed to avoid this problem; however the influence of chain like aggregation angle with respect to the magnetic gradient is more difficult to assess when using this disposition.

6.2 Data acquisition software

The tracking software presented here can be used to estimate the response of the magnetic microcarriers when used in conjunction with the magnetophoretic chamber described. There is room for improvement in the pre-filtering process and in the tracking process. The motion estimation model used for tracking magnetic microcarrier aggregations is very simple, but performs its task of allowing the estimation of the deflection pattern. The use of contextual information allows a better performance than the use of the general purpose tracking application used initially.

The initial established problem for this project was to design a device capable of allowing the collection of data on the magnetic response of therapeutic and/or diagnostic microcarriers when used in MRN. The first step to propose a solution to an engineering problem is to understand the nature of it. When the nature of the problem is clear, it is possible to decide if the use of computer science tools is useful to its solution or not. The screening work presented up to this point has allowed us to better understand the implications of the measurement of magnetophoretic attributes of therapeutic and/or diagnostic microcarriers.

The MRN system is expected to be composed basically by three main data source modules, plus a core software module [48]. The first data source is the physiological data, including blood

flows, pre-recorded images of the vasculature surrounding the target zone, etc. The second source of data is the system data related mainly to propulsion capacities of the system. Finally, the third source of data is the magnetic microcarriers database. The MRN system is expected to operate accessing this data sources to provide the medical team with all the resources needed to perform a MRN intervention.

This project can provide insights on the way in which the magnetic therapeutic/diagnostic microcarriers database can be designed and populated. Next generation of the data acquisition software developed for this thesis must include a step to retrieve information on magnetic navigable entities as: microcarrier identification, microcarrier magnetic content, microcarrier therapeutic agent identification, microcarrier therapeutic content and microcarrier size among others. After performing magnetophoretic experiences, the data acquisition software should generate data on magnetophoretic velocity, and the ratio of aggregated and unaggregated magnetic microparticles, as a very minimum. All this information is to be saved in a database and could be used to feed a theoretical model to determine the best route to reach the target, estimate the MRN intervention expected efficiency and help the medical team in selecting the appropriate therapeutic entity for a given patient. The present work can be used as the base for building such a complete platform to characterize any potential therapeutic and/or diagnostic microentity.

CHAPTER 7 CONCLUSION

The aim of this project was to design and test a device to allow the characterization of the deflection patterns of magnetic microentities intended for diagnostic and/or therapeutic targeted interventions. A microfluidic chamber was designed and preliminary results were presented. The magnetophoretic chamber designed allowed the observation of the movement of chain-like magnetic microparticle aggregations of around 200 μm in size.

In Chapter 2 the literature review is presented. A basic theoretical background on magnetophoresis and the application of magnetophoresis in magnetic manipulation is initially presented. Next the MRN technique as a novel cancer treatment alternative is presented, putting emphasis on the fact that magnetic microcarriers trajectory experimental studies, to our best knowledge, have not been performed up to now. Finally the common techniques used for tracking particles while moving in a flow are presented.

In Chapter 3 the methodology used in this research project is outlined. The microfluidics design is presented with some details; the simulation framework is explained jointly with the expected results from magnetophoretic experiences based on its results. Experimental results that are part of a conference paper are summarized. Finally the reasons for use OpenCV and Qt are explained.

A preliminary framework for tracking and data acquisition of magnetophoretic attributes is presented in Chapter 4. The initial exploration of the OpenCV blobtrack application, used in other project in the laboratory, is the main subject of this chapter. The results were promissory, even though there are problems with this tracking tool.

Taking into account the results obtained with the blobtrack application, a simple tracking software based in a translational model is proposed and applied to videos used in [10]. This simple tracking program shows better performance when compared with the OpenCV blobtrack sample application and is presented in Chapter 5.

In Chapter 6 the possible improvements at the experimental setup level are discussed. Some of the design decisions presented in Chapter 3 are reviewed, mainly regarding the positioning of the input inlet and the use of several outputs. It is also discussed the use of higher viscosity

liquids as transport fluid in order to avoid sedimentation. The validity of the assumption that using magnetphoretic velocity results in fluid flow of known viscosity can be used to estimate magnetophoretic velocity in blood is investigated. At the software level, this chapter puts the developed software in perspective with respect to the whole MRN system.

The work of this project could be extended in several directions:

- Repeating the experiences presented in [10] by using higher viscosity fluid and lower fluid flow speeds. By using neutrally buoyant particles it could be possible to evaluate the accuracy of fluid flow speeds and laminarity of the flow.
- Performing deflection experiences using the upgraded MRN platform [96] to generate propulsion forces in different angles with respect to the chain-like aggregations.
- Performing experiences with a magnetophoretic chamber having several outputs in order to estimate aggregation size distributions.
- Improving the tracking tool to detect individual particles.

This work is inserted in the MR Sub project, and so, the broader goal of it is to provide the basis for future developments allowing the design and implementation of a magnetic navigable microentities database. The use of the magnetophoretic chamber design and the development of improvements in the data acquisition software can provide a way to characterize any potential therapeutic microcarrier. We expect this work will be useful to open new ways for future investigations of magnetic response of therapeutic/diagnosis microagents in order to better plan future MRN interventions.

REFERENCES

[1] A. Nacev, A. Komaee, A. Sarwar, R. Probst, S. Kim, M. Emmert-Buck, and B. Shapiro, "Towards control of magnetic fluids in patients: Directing therapeutic nanoparticles to disease locations," *Control Systems, IEEE*, vol. 32, no. 3, pp. 32–74, 2012.

[2] A. Trafton, "The past, present and future of cancer," 2011, web.mit.edu/newsoffice/2011/-cancer-symposium-0318.html.

[3] S. Martel, J. Mathieu, O. Felfoul, A. Chanu, E. Aboussouan, S. Tamaz, P. Pouponneau, L. Yahia, G. Beaudoin, G. Soulez *et al.*, "Automatic navigation of an untethered device in the artery of a living animal using a conventional clinical magnetic resonance imaging system," *Applied Physics Letters*, vol. 90, no. 11, pp. 114105–114105, 2007.

[4] P. Pouponneau, J. Leroux, G. Soulez, L. Gaboury, and S. Martel, "Co-encapsulation of magnetic nanoparticles and doxorubicin into biodegradable microcarriers for deep tissue targeting by vascular MRI navigation," *Biomaterials*, vol. 32, no. 13, pp. 3481–3486, 2011.

[5] P. Pouponneau, J. Leroux, and S. Martel, "Magnetic nanoparticles encapsulated into biodegradable microparticles steered with an upgraded magnetic resonance imaging system for tumor chemoembolization," *Biomaterials*, vol. 30, no. 31, pp. 6327–6332, 2009.

[6] J. Mathieu and S. Martel, "Steering of aggregating magnetic microparticles using propulsion gradients coils in an MRI scanner," *Magnetic Resonance in Medicine*, vol. 63, no. 5, pp. 1336–1345, 2010.

[7] X. Zhao and L. Helseth, "Magnetophoresis of microspheres covered by magnetic nanoparticles," *Journal of Applied Physics*, vol. 102, no. 5, pp. 054905–054905, 2007.

[8] K. Peng, "Design and implementation of a fuzzy controller for steering microparticles inside blood vessels by using a MRI system," Master's thesis, École Polytechnique de Montréal, 2012.

[9] "Particle System Toolbox [Online]," http://www.mathworks.com/matlabcentral/-fileexchange/14314-particle-system-toolbox.

[10] G. Vidal and S. Martel, “Measuring the magnetophoretic characteristics of magnetic agents for targeted diagnostic or therapeutic interventions in the vascular network,” *Journal of Micro-Bio Robotics*, 2013.

[11] S. Gill, C. Malone, and M. Downing, “Magnetic susceptibility measurements of single small particles,” *Review of Scientific Instruments*, vol. 31, no. 12, pp. 1299–1303, 1960.

[12] N. A. Spaldin, *Magnetic materials: fundamentals and applications*, 2nd ed. Cambridge University Press, 2010.

[13] E. Purcell, *Electricity and magnetism*, 2nd ed. Cambridge University Press, 2011.

[14] M. Zborowski, L. Sun, L. R. Moore, P. Stephen Williams, and J. J. Chalmers, “Continuous cell separation using novel magnetic quadrupole flow sorter,” *Journal of Magnetism and Magnetic Materials*, vol. 194, no. 1, pp. 224–230, 1999.

[15] M. Dimaki and W. E. Svendsen, *Micro and Nano Techniques for the Handling of Biological Samples*. CRC Press, 2011, ch. 7. Magnetic Manipulation of Biological Structures, pp. 173–196.

[16] H. Bruus, *Theoretical Microfluidics*, ser. Oxford Master Series in Physics. OUP Oxford, 2008.

[17] S. Reddy, L. Moore, L. Sun, M. Zborowski, and J. Chalmers, “Determination of the magnetic susceptibility of labeled particles by video imaging,” *Chemical engineering science*, vol. 51, no. 6, pp. 947–956, 1996.

[18] A. Adamczyk and L. Rimai, “2-dimensional particle tracking velocimetry (PTV): technique and image processing algorithms,” *Experiments in fluids*, vol. 6, no. 6, pp. 373–380, 1988.

[19] J. J. Chalmers, S. Haam, Y. Zhao, K. McCloskey, L. Moore, M. Zborowski, P. S. Williams *et al.*, “Quantification of cellular properties from external fields and resulting induced velocity: cellular hydrodynamic diameter,” *Biotechnology and bioengineering*, vol. 64, no. 5, pp. 509–518, 1999.

[20] J. J. Chalmers, S. Haam, Y. Zhao, K. McCloskey, L. Moore, M. Zborowski, P. S. Williams *et al.*, “Quantification of cellular properties from external fields and resulting induced

velocity: magnetic susceptibility," *Biotechnology and bioengineering*, vol. 64, no. 5, pp. 519–526, 1999.

[21] J. Chalmers, Y. Zhao, M. Nakamura, K. Melnik, L. Lasky, L. Moore, and M. Zborowski, "An instrument to determine the magnetophoretic mobility of labeled, biological cells and paramagnetic particles," *Journal of magnetism and magnetic materials*, vol. 194, no. 1, pp. 231–241, 1999.

[22] L. R. Moore, H. Fujioka, P. S. Williams, J. J. Chalmers, B. Grimberg, P. A. Zimmerman, and M. Zborowski, "Hemoglobin degradation in malaria-infected erythrocytes determined from live cell magnetophoresis," *The FASEB journal*, vol. 20, no. 6, pp. 747–749, 2006.

[23] U. Häfeli, M. Lobedann, J. Steingroewer, L. Moore, and J. Riffle, "Optical method for measurement of magnetophoretic mobility of individual magnetic microspheres in defined magnetic field," *Journal of magnetism and magnetic materials*, vol. 293, no. 1, pp. 224–239, 2005.

[24] B. Kashevsky, A. Zholud, and S. Kashevsky, "Magnetophoretic trajectory tracking magnetometry: A new technique for assessing magnetic properties of submagnetic microparticles and cells," *Review of Scientific Instruments*, vol. 83, no. 7, pp. 075104–075104, 2012.

[25] M. Suwa and H. Watarai, "Magnetophoretic velocimetry of manganese (ii) in a single emulsion droplet at the femtomole level," *Analytical chemistry*, vol. 73, no. 21, pp. 5214–5219, 2001.

[26] M. Suwa and H. Watarai, "Magnetophoretic velocimetry of manganese (ii) in a single microdroplet in a flow system under a high gradient magnetic field generated with a superconducting magnet," *Analytical chemistry*, vol. 74, no. 19, pp. 5027–5032, 2002.

[27] M. Suwa and H. Watarai, "Magnetophoretic velocity of microorganic droplets adsorbed by dysprosium (iii) laurate in water," *Journal of Chromatography A*, vol. 1013, no. 1, pp. 3–8, 2003.

[28] S. Egami and H. Watarai, "Magnetic susceptibility measurement of a microdroplet interface using a magnetic circuit," *Analyst*, vol. 134, no. 2, pp. 278–282, 2009.

[29] C. Wilhelm, F. Gazeau, J. Bacri *et al.*, "Magnetophoresis and ferromagnetic resonance of magnetically labeled cells," *European Biophysics Journal*, vol. 31, no. 2, pp. 118–125, 2002.

[30] Y. Jing, N. Mal, P. S. Williams, M. Mayorga, M. S. Penn, J. J. Chalmers, and M. Zborowski, “Quantitative intracellular magnetic nanoparticle uptake measured by live cell magnetophoresis,” *The FASEB Journal*, vol. 22, no. 12, pp. 4239–4247, 2008.

[31] X. Jin, Y. Zhao, A. Richardson, L. Moore, P. S. Williams, M. Zborowski, and J. J. Chalmers, “Differences in magnetically induced motion of diamagnetic, paramagnetic, and superparamagnetic microparticles detected by cell tracking velocimetry,” *Analyst*, vol. 133, no. 12, pp. 1767–1775, 2008.

[32] M. A. Gijs, F. Lacharme, and U. Lehmann, “Microfluidic applications of magnetic particles for biological analysis and catalysis,” *Chemical reviews*, vol. 110, no. 3, pp. 1518–1563, 2010.

[33] A. A. S. Bhagat, H. Bow, H. W. Hou, S. J. Tan, J. Han, and C. T. Lim, “Microfluidics for cell separation,” *Medical and Biological Engineering and Computing*, vol. 48, no. 10, pp. 999–1014, 2010.

[34] J. Watson, “Magnetic filtration,” *Journal of Applied Physics*, vol. 44, no. 9, pp. 4209–4213, 1973.

[35] J. Oberteuffer, “High gradient magnetic separation,” *Magnetics, IEEE Transactions on*, vol. 9, no. 3, pp. 303–306, 1973.

[36] S. Miltenyi, W. Müller, W. Weichel, and A. Radbruch, “High gradient magnetic cell separation with MACS,” *Cytometry*, vol. 11, no. 2, pp. 231–238, 1990.

[37] M. A. Gijs, “Magnetic bead handling on-chip: new opportunities for analytical applications,” *Microfluidics and Nanofluidics*, vol. 1, no. 1, pp. 22–40, 2004.

[38] N. Pamme, “Magnetism and microfluidics,” *Lab on a Chip*, vol. 6, no. 1, pp. 24–38, 2006.

[39] N. Pamme and A. Manz, “On-chip free-flow magnetophoresis: continuous flow separation of magnetic particles and agglomerates,” *Analytical chemistry*, vol. 76, no. 24, pp. 7250–7256, 2004.

[40] N. Pamme, J. C. Eijkel, and A. Manz, “On-chip free-flow magnetophoresis: Separation and detection of mixtures of magnetic particles in continuous flow,” *Journal of magnetism and magnetic materials*, vol. 307, no. 2, pp. 237–244, 2006.

[41] N. Pamme and C. Wilhelm, “Continuous sorting of magnetic cells via on-chip free-flow magnetophoresis,” *Lab Chip*, vol. 6, no. 8, pp. 974–980, 2006.

[42] M. Vojtšek, M. D. Tarn, N. Hirota, and N. Pamme, “Microfluidic devices in superconducting magnets: on-chip free-flow diamagnetophoresis of polymer particles and bubbles,” *Microfluidics and Nanofluidics*, pp. 1–11, 2012.

[43] E. Furlani and Y. Sahoo, “Analytical model for the magnetic field and force in a magnetophoretic microsystem,” *Journal of Physics D: Applied Physics*, vol. 39, no. 9, p. 1724, 2006.

[44] E. Furlani, Y. Sahoo, K. Ng, J. Wortman, and T. Monk, “A model for predicting magnetic particle capture in a microfluidic bioseparator,” *Biomedical Microdevices*, vol. 9, no. 4, pp. 451–463, 2007.

[45] E. P. Furlani and X. Xue, “A model for predicting field-directed particle transport in the magnetofection process,” *Pharmaceutical research*, vol. 29, no. 5, pp. 1366–1379, 2012.

[46] S. A. Khashan and E. P. Furlani, “Coupled particle–fluid transport and magnetic separation in microfluidic systems with passive magnetic functionality,” *Journal of Physics D: Applied Physics*, vol. 46, no. 12, p. 125002, 2013.

[47] L. A. Sasso, I. H. Johnston, M. Zheng, R. K. Gupte, A. Ündar, and J. D. Zahn, “Automated microfluidic processing platform for multiplexed magnetic bead immunoassays,” *Microfluidics and Nanofluidics*, pp. 1–10, 2012.

[48] S. Martel and M. Vonthron, “Interactive system for medical interventions based on magnetic resonance targeting,” in *ACHI 2011, The Fourth International Conference on Advances in Computer-Human Interactions*, 2011, pp. 197–201.

[49] J. Mathieu, S. Martel, L. Yahia, G. Soulez, G. Beaudoin *et al.*, “Preliminary investigation of the feasibility of magnetic propulsion for future microdevices in blood vessels,” *BioMedical Materials and Engineering*, vol. 15, no. 5, p. 367, 2005.

[50] J. Mathieu, G. Beaudoin, and S. Martel, “Method of propulsion of a ferromagnetic core in the cardiovascular system through magnetic gradients generated by an MRI system,” *Biomedical Engineering, IEEE Transactions on*, vol. 53, no. 2, pp. 292–299, 2006.

[51] J.-B. Mathieu and S. Martel, “Magnetic microparticle steering within the constraints of an MRI system: proof of concept of a novel targeting approach,” *Biomedical microdevices*, vol. 9, no. 6, pp. 801–808, 2007.

[52] J. Mathieu and S. Martel, “Aggregation of magnetic microparticles in the context of targeted therapies actuated by a magnetic resonance imaging system,” *Journal of Applied Physics*, vol. 106, no. 4, p. 044904, 2009.

[53] P. Vartholomeos, C. Mavroidis, and N. Hata, “Magnetic targeting of aggregated nanoparticles for advanced lung therapies: A robotics approach,” in *Biomedical Robotics and Biomechatronics (BioRob), 2010 3rd IEEE RAS and EMBS International Conference on*. IEEE, 2010, pp. 861–868.

[54] P. Vartholomeos and C. Mavroidis, “Simulation platform for self-assembly structures in MRI-guided nanorobotic drug delivery systems,” in *Robotics and Automation (ICRA), 2010 IEEE International Conference on*. IEEE, 2010, pp. 5594–5600.

[55] P. Vartholomeos and C. Mavroidis, “In-silico studies of micro magnetic particle aggregations in fluid environments for MRI guided drug delivery,” *IEEE Transactions on Biomedical Engineering*, vol. 59, no. 11, pp. 3028–3038, 2012.

[56] J. Riegler, J. Wells, P. Kyrtatos, A. Price, Q. Pankhurst, and M. Lythgoe, “Targeted magnetic delivery and tracking of cells using a magnetic resonance imaging system,” *Biomaterials*, vol. 31, no. 20, pp. 5366–5371, 2010.

[57] J. Riegler, B. Allain, R. Cook, M. Lythgoe, and Q. Pankhurst, “Magnetically assisted delivery of cells using a magnetic resonance imaging system,” *Journal of Physics D: Applied Physics*, vol. 44, no. 5, p. 055001, 2011.

[58] A. Yilmaz, O. Javed, and M. Shah, “Object tracking: A survey,” *Acm Computing Surveys (CSUR)*, vol. 38, no. 4, p. 13, 2006.

[59] E. Meijering, O. Dzyubachyk, and I. Smal, “Methods for cell and particle tracking,” *Methods in Enzymology: Live Cell Imaging*, 2012.

[60] S. Vishwakarma and A. Agrawal, “A survey on activity recognition and behavior understanding in video surveillance,” *The Visual Computer*, pp. 1–27, 2012.

[61] R. Parthasarathy, “Rapid, accurate particle tracking by calculation of radial symmetry centers,” *Nature Methods*, vol. 9, no. 7, pp. 724–726, 2012.

[62] J. Shi and C. Tomasi, “Good features to track,” in *Computer Vision and Pattern Recognition, 1994. Proceedings CVPR’94., 1994 IEEE Computer Society Conference on*. IEEE, 1994, pp. 593–600.

[63] J. Santiago, S. Wereley, C. Meinhart, D. Beebe, and R. Adrian, “A particle image velocimetry system for microfluidics,” *Experiments in fluids*, vol. 25, no. 4, pp. 316–319, 1998.

[64] M. Raffel, C. E. Willert, S. T. Wereley, and J. Kompenhans, *Particle image velocimetry: a practical guide*. Springer, 2007.

[65] P. Ruhnau, C. Guetter, T. Putze, and C. Schnörr, “A variational approach for particle tracking velocimetry,” *Measurement Science and Technology*, vol. 16, no. 7, p. 1449, 2005.

[66] Y.-C. Lei, W.-H. Tien, J. Duncan, M. Paul, N. Ponchaut, C. Mouton, D. Dabiri, T. Rösgen, and J. Hove, “A vision-based hybrid particle tracking velocimetry (PTV) technique using a modified cascade correlation peak-finding method,” *Experiments in fluids*, vol. 53, no. 5, pp. 1251–1268, 2012.

[67] M. Zborowski, J. Chalmers, and L. R. Moore, “Method for determining particle characteristics,” US Patent 5,974,901, Nov. 2, 1999, uS Patent 5,974,901.

[68] C. Cierpka, B. Lütke, and C. J. Kähler, “Higher order multi-frame particle tracking velocimetry,” *Experiments in Fluids*, vol. 54, no. 5, pp. 1–12, 2013.

[69] J. B. Mathieu, “Étude des paramètres physiques en vue d’applications médicales de l’actionnement magnétique de dispositifs médicaux par un système d’imagerie par résonance magnétique,” Ph.D. dissertation, École Polytechnique de Montréal, 2009.

[70] G. Vidal and S. Martel, “Characterization by magnetophoresis of therapeutic microcarriers relying on embedded nanoparticles to allow navigation in the vascular network,” in *Manipulation, Manufacturing and Measurement on the Nanoscale (3M-NANO), 2012 International Conference on*, 2012, pp. 54–58.

[71] “The OpenCV Video Surveillance / Blob Tracker Facility [Online],” http://-opencv.willowgarage.com/wiki/VideoSurveillance.

[72] B. J. Nelson, I. K. Kaliakatsos, and J. J. Abbott, “Microrobots for minimally invasive medicine,” *Annual Review of Biomedical Engineering*, vol. 12, pp. 55–85, 2010.

[73] G. H. Hübner, N. Steudel, G. Kleber, C. Behrmann, E. Lotterer, and W. E. Fleig, “Hepatic arterial blood flow velocities: assessment by transcutaneous and intravascular doppler sonography,” *Journal of hepatology*, vol. 32, no. 6, pp. 893–899, 2000.

[74] C. Tziafalia, M. Vlychou, K. Tepetes, N. Kelekis, and I. V. Fezoulidis, “Echo-doppler measurements of portal vein and hepatic artery in asymptomatic patients with hepatitis B virus and healthy adults,” *Journal of Gastrointestinal and Liver Diseases*, vol. 15, no. 4, p. 343, 2006.

[75] J. Li, D. Chen, and G. Chen, “Low-temperature thermal bonding of PMMA microfluidic chips,” *Analytical letters*, vol. 38, no. 7, pp. 1127–1136, 2005.

[76] K. Peng and S. Martel, “Preliminary design of a SIMO fuzzy controller for steering microparticles inside blood vessels by using a magnetic resonance imaging system,” in *Engineering in Medicine and Biology Society, EMBC, 2011 Annual International Conference of the IEEE*. IEEE, 2011, pp. 920–923.

[77] Y. Sun, Y. C. Kwok, and N.-T. Nguyen, “Low-pressure, high-temperature thermal bonding of polymeric microfluidic devices and their applications for electrophoretic separation,” *Journal of Micromechanics and Microengineering*, vol. 16, no. 8, p. 1681, 2006.

[78] R. T. Kelly and A. T. Woolley, “Thermal bonding of polymeric capillary electrophoresis microdevices in water,” *Analytical chemistry*, vol. 75, no. 8, pp. 1941–1945, 2003.

[79] G. Bringout, “Actionneur pour le guidage de micro-particules magnétiques et thérapeutiques dans le systéme vasculaire : bobines de gradients pulsés pour des essaes pré-cliniques,” Master’s thesis, École Polytechnique de Montréal, 2011.

[80] L. F. Moody, “Friction factors for pipe flow,” *Trans. Asme*, vol. 66, no. 8, pp. 671–684, 1944.

[81] M. Suwa and H. Watarai, “Magnetoanalysis of micro/nanoparticles: a review,” *Analytica chimica acta*, vol. 690, no. 2, pp. 137–147, 2011.

[82] “OpenSource Computer Vision,” http://opencv.org/.

[83] T. P. Chen, H. Haussecker, A. Bovyrin, R. Belenov, K. Rodyushkin, A. Kuranov, and V. Eruhimov, “Computer vision workload analysis: Case study of video surveillance systems,” *Intel Technology Journal*, vol. 9, no. 2, pp. 109–118, 2005.

[84] A. Senior, A. Hampapur, Y.-L. Tian, L. Brown, S. Pankanti, and R. Bolle, “Appearance models for occlusion handling,” *Image and Vision Computing*, vol. 24, no. 11, pp. 1233–1243, 2006.

[85] C. Carr, M. Espy, P. Nath, S. L. Martin, M. D. Ward, and J. Martin, “Design, fabrication and demonstration of a magnetophoresis chamber with 25 output fractions,” *Journal of magnetism and magnetic materials*, vol. 321, no. 10, pp. 1440–1445, 2009.

[86] L. Li, W. Huang, I. Y. Gu, and Q. Tian, “Foreground object detection from videos containing complex background,” in *Proceedings of the eleventh ACM international conference on Multimedia*. ACM, 2003, pp. 2–10.

[87] S. Suzuki *et al.*, “Topological structural analysis of digitized binary images by border following,” *Computer Vision, Graphics, and Image Processing*, vol. 30, no. 1, pp. 32–46, 1985.

[88] D. Comaniciu, V. Ramesh, and P. Meer, “Real-time tracking of non-rigid objects using mean shift,” in *Computer Vision and Pattern Recognition, 2000. Proceedings. IEEE Conference on*, vol. 2. IEEE, 2000, pp. 142–149.

[89] K. Nummiaro, E. Koller-Meier, L. Van Gool *et al.*, “A color-based particle filter,” in *First International Workshop on Generative-Model-Based Vision*, vol. 2002. Citeseer, 2002, p. 01.

[90] “Qt, cross-platform application and UI framework,” http://qt.digia.com.

[91] M. S. Sakar, E. B. Steager, A. A. Julius, M. Kim, V. Kumar, G. J. Pappas *et al.*, “Modeling, control and experimental characterization of microbiorobots,” *The International Journal of Robotics Research*, vol. 30, no. 6, pp. 647–658, 2011.

[92] E. Loth, “Drag of non-spherical solid particles of regular and irregular shape,” *Powder Technology*, vol. 182, no. 3, pp. 342–353, 2008.

[93] N.-S. Cheng, “Formula for the viscosity of a glycerol-water mixture,” *Industrial & engineering chemistry research*, vol. 47, no. 9, pp. 3285–3288, 2008.

[94] T. M. Squires and S. R. Quake, “Microfluidics: Fluid physics at the nanoliter scale,” *Reviews of modern physics*, vol. 77, no. 3, p. 977, 2005.

[95] C. Mikkelsen, M. Fougt Hansen, and H. Bruus, “Theoretical comparison of magnetic and hydrodynamic interactions between magnetically tagged particles in microfluidic systems,” *Journal of Magnetism and Magnetic Materials*, vol. 293, no. 1, pp. 578–583, 2005.

[96] M. Vonthron, V. Lalande, G. Bringout, C. Tremblay, and S. Martel, “A MRI-based integrated platform for the navigation of micro-devices and microrobots,” in *Intelligent Robots and Systems (IROS), 2011 IEEE/RSJ International Conference on*. IEEE, 2011, pp. 1285–1290.

APPENDIX 1– Rod model for chain-like magnetic aggregations

One of the ways in which chain-like magnetic aggregations is approximated is by using a rod like representation.

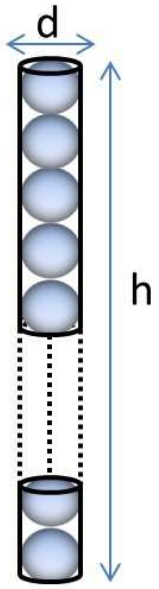

In the figure shown at the side the chain-like magnetic aggregation of n equal size particles is represented. Due to the fact that we know that all particles have the same size, we get:

$$h = nd \qquad \text{Ann1-1}$$

The volume of a cylinder (a rod) is:

$$V = \pi r^2 h \qquad \text{Ann1-2}$$

with $r = d/2$. Then the volume of the chain-like aggregation in terms of the diameter of their constituent particles is:

$$V = \frac{n}{4}\pi d^3 \qquad \text{Ann1-3}$$

A sphere with an equivalent volume is

$$V = \frac{4}{3}\pi {r_{eq}}^3 \qquad \text{Ann1-4}$$

and $r_{eq} = d_{eq}/2$ we have that

$$V = \frac{1}{6}\pi {d_{eq}}^3 \qquad \text{Ann1-5}$$

By equalizing Eq. Ann1-3 and Eq. Ann1-5, the diameter of the equivalent sphere is obtained:

$$d_{eq} = \sqrt[3]{\frac{3}{2}n}\, d \qquad \text{Ann1-6}$$

In the simulation case, $n = 280$ and $d = 41.13 \times 10^{-6}$ m with which we obtain an equivalent diameter of $d_{eq} = 308.017 \times 10^{-6}$ m.